ANL/ESD-17/26

Impact of Distributed Energy Resources on the Bulk Energy System

Combined Modeling of Transmission and Distribution Systems and Benchmark Case Studies

Energy Systems Division

ANL/ESD-17/26

Impact of Distributed Energy Resources on the Bulk Energy System

Combined Modeling of Transmission and Distribution Systems and Benchmark Case Studies

Prepared by:
Ning Kang and Ravindra Singh
Argonne National Laboratory

James T. Reilly
Reilly Associates

Nicole Segal
North American Electric Reliability Corporation

Prepared for:
U.S. Department of Energy, Office of Electricity Delivery and Energy Reliability

November 2017

CONTENTS

CONTENTS (CONT.)

FIGURES

FIGURES (CONT.)

TABLES

TABLES (CONT.)

ACRONYMS

AGC	Automatic Generation Control
BES	Bulk Energy System
BESS	Battery Energy Storage System
CMPLDWG	Composite Load Model with Distributed PV
DER	Distributed Energy Resource
DFIG	Doubly Fed Induction Generator
DFT	Discrete Fourier Transform
EKF	Extended Kalman Filter
EM	Expectation-Maximization
EMT	Electromagnetic Transient
FERC	Federal Energy Regulatory Commission
GSC	Grid-Side Converter
IGBT	Insulated Gate Bipolar Transistor
KF	Kalman Filter
NERC	North American Electric Reliability Corporation
PCC	Point of Common Coupling
PI	Proportional Integral
PSS	Power System Stabilizer
PV	Photovoltaic
ROCOF	Rate of Change of Frequency
RSC	Rotor-Side Converter
SG	Synchronous Generator
T-D	Transmission to Distribution
T&D	Transmission and Distribution
TSR	Tip Speed Ratio
VA	Volt-Ampere
WECC	Western Electricity Coordinating Council
WTG	Wind Turbine Generator

ACKNOWLEDGMENTS

This report was prepared by UChicago Argonne, LLC, operator of Argonne National Laboratory. Argonne's work was supported by the U.S. Department of Energy (DOE) under contract DE-AC02-06CH11357.

The authors wish to acknowledge the sponsorship and guidance provided by Dan Ton of the U.S. DOE Office of Electricity Delivery and Energy Reliability. We would also like to acknowledge the guidance and insights provided by Jianhui Wang of Argonne National Laboratory throughout the project. Lastly, we would like to extend our special appreciation to Thomas Coleman of NERC, who we engaged with and interacted with as part of this project for his valuable suggestions and feedback.

This page intentionally left blank.

EXECUTIVE SUMMARY

The high penetration of distributed energy resources (DERs) on modern distribution systems introduces intermittent power generation, stochastic system operating conditions, and bi-directional power flows that impact the system responses to various types of disturbances and may pose challenges to the operations and reliability of the Bulk Energy System (BES). In order to understand the impact of DERs on the planning and operation of the BES, the distribution system can no longer be represented as a single load at a node on the transmission system. At the same time, advanced control capabilities of DERs offer potential opportunities for improving BES reliability by transforming DERs from a passive "do no harm" resource to an active "support reliability" resource when applied in a planned and well-thought-out manner. This concept is often described as DER "flexibility." With the persistent trend towards a high-penetration of DERs in distribution systems, regulators such as the North American Electric Reliability Corporation (NERC), planning coordinators and grid operators are in serious need of understanding the full-spectrum impact of DERs on the BES to ensure secure and reliable grid planning and operations.

To that end, a combined model of transmission and distribution systems (hereafter called "T&D combined model") was developed on the MATLAB/Simulink platform. The model for the transmission system was selected to faithfully represent all the operation modes and dynamics of bulk energy systems. Similarly, the distribution system was modeled with high penetration of multiple types of DERs, along with interconnection standard implemented in accordance with IEEE Std. 1547. This model is capable of full-scale static, dynamic and electromagnetic-transient (EMT) simulations. Three-phase and single-phase DER modeling was developed and integrated into the distribution network. With these features, the T&D combined model can be used by grid planners and operators to evaluate the aggregate effects of unbalanced multi-phase DERs on the transmission-to-distribution (T-D) interface, understand the level of impact of DERs on the BES reliability, and evaluate advanced control strategies to improve BES performance.

Another gap identified is that a paradigm shift is needed for BES planning and operation studies. The emergence of high-penetration DERs necessitates new considerations in conventional BES steady-state and dynamic analysis. Revision is needed for BES studies to factor in the impact of DERs' interconnection requirements such as ride-through and islanding, and their advanced control capabilities to properly represent the dynamic behavior of DERs. In close collaboration with the NERC's Essential Reliability Service Working Group and Distributed Energy Resources Task Force, six BES benchmark case studies were carried out using the developed T&D combined model. The objective is to provide a guideline and benchmark in analyzing the reliability impact on modern BES featured by high-penetration DERs. These benchmark case studies cover DERs' impact on the voltage stability, frequency regulation, and dynamic stability of a BES, and are listed as follows:

1. Effect of DERs replacing synchronous machines on inertial and primary frequency responses of a BES;

2. Impact of DERs on automatic generation control (AGC);

3. Impact of DERs on load following of a BES;

4. Effect of intermittent DER output on system voltages and frequency;

5. DER impact on the small-signal stability of a BES;

6. DER impact on the transient stability of a BES.

Key findings from these analyses showed that increasing DER penetration level tends to degrade the BES reliability and provided insights into mitigation strategies.

It is further realized that NERC, planning coordinators and grid operators need a real-world tool for routine planning and operations studies for high-DER-penetration scenarios and handle practical scenarios on actual T&D networks. However, the T&D combined model developed in this work cannot be scaled to a level of network size that is realistic and meets the computational requirements of the BES, owing to MATLAB's inherent limitations. To overcome these challenges, two approaches can be taken. The first one is to develop a combined T&D model on another platform other than MATLAB/Simulink which can address the network size and computational complexity issues. In this approach, both transmission and distribution systems are modeled on the same platform and there is no need for information exchange mainly because the combined system is solved simultaneously as one system. However, this approach is highly complex and time-consuming.

Another approach falls into the category of T&D co-simulation. In this approach, the transmission and distribution systems are simulated using two independent platforms and these two platforms exchange data between each other in a cyclical manner. Based on the exchanged data, each system (T or D) is solved independently. The data exchange between the two systems continues until both the systems converge. Since mature transmission or distribution simulation tool each is specialized in modeling and simulating real-world networks, integrating them together in one tool provides a practical means to enable day-to-day planning and operations studies for high-DER-penetration scenarios and handling real-life scenarios on actual T&D networks for NERC, planning coordinators, and grid operators.

Given the urgency of the problem at hand and available options, a T&D co-simulation tool, potentially coupling PSS®E and EMTP, will be developed in the next phase of this project. Once developed, it can underpin applications that facilitate risk-reduction in planning and operation and help improve operational efficiencies that may benefit various stakeholders across T&D.

1 INTRODUCTION

Stimulated by ambitious state legislature and incentives, and rapid technological progress driving price down, industries are increasingly adopting distributed renewable resources (DERs) in their generation portfolio. New York, Oregon, and the District of Columbia expanded their mandates for renewable generation to reach 50% of their total electricity generation by 2030, 2032, and 2040, respectively [1]. The California Energy Commission stipulates that publicly owned utilities procure half of the state's electricity from renewable sources by 2030 [2]. As DERs continue to penetrate into the grid, the followed technical problems and reliability challenges emerge, which if not addressed promptly will hinder wide deployment of DERs.

In the past decades, challenges and solutions with respect to DER integration into distribution grid were the centerpiece of the research and development effort. DERs' impact on the bulk energy system (BES) were largely ignored. However, in recent years influences on the BES caused by high DER penetration in the distribution system have become more obvious and pressing. First and foremost, the high penetration of DERs on distribution systems introduces intermittent power generation, stochastic system operating conditions, and bi-directional power flows that impact the system responses to various types of disturbances and may pose challenges to the operations and reliability of the BES. Therefore, it is imperative for regulators such as North American Electric Reliability Corporation (NERC), planning coordinators and grid operators to fully understand the reliability impact of high penetration DERs on the BES and ensure secure and reliable grid planning and operations.

In an attempt to assist interested entities in grasping the full-spectrum impact of high-penetration DERs on the BES, gaps in existing modeling and analysis approaches are identified and the corresponding solutions are proposed in this report. Traditionally, for BES planning and operation studies, the distribution system is represented as a single static load at a transmission node, where generation is netted with load. Clearly this is not suitable for highly active distribution systems with a high penetration of DERs. To fill this gap, a transmission and distribution (T&D) combined model was developed on the MATLAB/Simulink platform in this report. The T&D combined model thoroughly models all the DERs (single-phase and three-phase) interconnected at the distribution grid which allows accurate study of their impacts on the bulk system power flows and dynamic performance.

It is also realized that a paradigm shift is needed for BES planning and operation studies due to the emergence of high-penetration DERs. New considerations are necessary for BES studies to factor in the impact of DERs' interconnection requirements such as ride-through and islanding, and their advanced control capabilities to properly represent the dynamic behavior of DERs. Motivated to provide a guideline in analyzing the reliability impact on modern BES featured by high DER penetration, six benchmark case studies were conducted using the developed T&D combined model in this report. These benchmark case studies cover DER's impact on the voltage stability, frequency regulation and dynamic stability of BES considering DER interconnection standards. Specifically,

- In benchmark case 1, "Effect of DERs replacing synchronous machines on inertial and primary frequency response of a BES," it was seen that overall transmission system inertia is reduced with an increase in DER replacement of synchronous generators (SGs). The higher the DER penetration, the higher the initial rate of change of frequency and the lower the frequency nadir upon the disturbance. Higher DER penetration can also result in lower settling frequency in the BES, indicating that it is more challenging for the primary frequency control of the responsive SGs to arrest the frequency deviation. Therefore, reduced system inertia may threaten BES stability, and mitigation measures to compensate lost inertia should be considered.

- In benchmark case 2, "Impact of DERs on AGC," the recovery time for the AGC to restore transmission system frequency increased with the level of DER penetration. For DER penetrations of 0%, 10%, 40%, and 70% in the Kundur Two-Area system, frequency restoration times were 40 s, 45 s, 55 s, and 70 s, respectively. It was also observed that larger and longer frequency oscillations occur upon the disturbance for higher-DER scenarios. The system's inability to quickly dampen these big swings could cause more equipment to trip off in order to protect itself and thus possibly lead to a cascading failure.

- In benchmark case 3, "Impact of DER on load following of a BES," it was demonstrated that high DER penetration also creates ramping challenges for the BES (commonly described as the "duck curve"). Corresponding to 10% and 50% photovoltaic penetration levels, the three-hour BES ramping from 5 to 8 pm increased from 717 MW to 1424 MW, i.e., almost doubled.

- In benchmark case 4, "Effect of intermittent DER output on system voltages and frequency," the effect of intermittent DER output on system voltage stabilities was investigated. In the worst-case scenarios, when the power output of the DERs is changing at a certain low frequency (for example, 0.5 Hz in the case study), oscillations of the corresponding frequency in system voltage and other measurements can be observed on the power grid. These low-frequency oscillations do not cause the DER protection system to trigger, nor are they damped by power system stabilizers. These low-frequency oscillations may amplify once a contingency event occurs and potentially cause the entire system to collapse.

- In benchmark case 5, "DER impact on the small-signal stability of a BES," the eigenvalues related to small-signal stability of a BES were studied. The eigenvalues tend to move to the right half of the s-plane with higher DER penetration, which makes the system more prone to instability caused by small disturbances. For the Kundur Two-Area system utilized in the case study, 30% DER penetration is enough to make the system small-signal unstable. This result does not imply that 30% DER penetration is the threshold to cause small-signal instability for all the systems under all the operating conditions,

but rather it should be treated as an indicative level of DER penetration that could cause a system small-signal unstable.

- In benchmark case 6, "DER impact on the transient stability of a BES," it was demonstrated that higher DER penetration conditions may lead to higher peak-to-peak oscillation values, faster DER tripping, and a longer time for the system to return to normal. In other words, more DER penetration may put the power grid at risk of instability after a severe transmission system fault.

The remainder of this report is organized as follows.

Chapter 2 documents the current practice of modeling distribution-system DERs for BES studies and understanding their impact on high-level analysis of BESs. An understanding and a gap analysis of the state of the art in DER modeling techniques provide guidance for DER modeling efforts for BES steady-state and dynamic studies.

Chapter 3 introduces the T&D combined model developed on the MATLAB/Simulink platform, taking into account the caveats identified in existing DER modeling techniques from the previous Chapter. This T&D combined model incorporates three-phase as well as single-phase DER modeling in the distribution system, which enables operators to understand the aggregate effects of the unbalanced multi-phase DERs on the transmission to distribution (T-D) interface with an appropriate level of spatial representation.

Chapter 4 describes the findings from a literature survey of various real-time frequency estimation and prediction techniques for sudden changes in system frequency due to intermittent DERs. On the basis of these estimation and prediction techniques, appropriate actions to provide frequency support are presented.

Chapter 5 presents the results of six benchmark case studies on the impact of DERs on frequency regulation, voltage stability, and dynamic stability of a BES, using the T&D combined model developed in this work.

Chapter 6 summarizes the results achieved in this work and lays out plans for future work on (a) impact analyses and reliability improvement strategies for BES considering high-penetration DERs on the distribution level; and (b) development of a real-world T&D co-simulation tool.

2 MODELING OF DERs FOR HIGH-LEVEL IMPACT ANALYSIS IN BESs

The distribution grid is becoming highly active, with a high penetration of DERs. Considering the significant impact of an active distribution grid on the bulk power system, it is no longer realistic to regard the distribution substation as a static passive load. It is desirable now to thoroughly model all the DERs interconnected at the distribution grid for bulk power system planning studies; however, the computational burden and dimension of the problem may be prohibitive for certain studies. Therefore, certain simplifications may be achieved by aggregating models with similar characteristics and/or using reduced-order dynamic equivalent models. There is a trade-off between modeling accuracy and modeling simplicity in order to represent the DERs with a sufficient level of detail to study their impacts on bulk system power flows and dynamic performance.

In this chapter, the impact of DER modeling on BES steady-state studies (power flow analysis and short-circuit analysis) and BES dynamic studies (disturbance ride-through studies and transient stability studies) is identified as well. When considering the impact of DER modeling on bulk power system planning studies, it is meaningful to differentiate different technology types, e.g., inverter-interfaced and rotational-machine-based DERs. In addition, the analysis should factor in the impact of interconnection requirements such as ride-through and islanding to represent the dynamic behavior among DERs using different types of generation. Moreover, differentiating DERs by resource type, e.g., dispatchable vs non-dispatchable, would help develop meaningful dispatch scenarios.

2.1 DER MODELING IMPACT ON STEADY-STATE STUDIES

This section mainly focuses on DER modeling's impact on BES steady-state studies, which include power flow studies and short-circuit studies.

2.1.1 DER Modeling Impact on Steady-State Power Flow Studies

Power flow analysis is used to determine bulk power system real and reactive power flows for network expansion planning, voltage stability studies, and coordination of voltage controls at the T&D interface. A power flow also initializes the state variables of a dynamic bulk system model for a dynamic stability study.

Modeling of DERs in these steady-state power flow studies would consider the real power injection at the distribution system level as well as the reactive power that may be provided by DERs. Usually, power flow calculations only require a standard generator or simplistic Norton or Thevenin equivalent with voltage control loops.

To capture the effect of reactive power support and the impact of DERs on voltage stability, aggregation of various DERs at the distribution substation is insufficient for steady-state power flow studies. In addition, when there is a high penetration of DERs injecting both

real power and reactive power, which are creating reverse power flows from distribution to the bulk system, a detailed representation of DERs is required.

For grid regions where DER performance requirements vary, different equivalent generator models may be used for each DER to appropriately reflect the DER performance. The inverter-based DER modeling for power flow analysis published in [3]–[5] assumes only positive-sequence DER representation for power flow analysis, which is not suitable for an unbalanced distribution grid with single-phase laterals.

Reference [6] presents steady-state sequence-component frame models of DER units for steady-state power flow studies. The proposed DER models include both the rotational-machine-based and inverter-based DER. In addition, both constant-power (P-Q) and regulated-voltage modes of DER operation are considered. In reference [7], the authors further extend the three-phase inverter-based DER model to the more prevalent single-phase inverter-based DERs for power flow studies.

2.1.2 DER Modeling Impact on Steady-State Short-Circuit Studies

Short-circuit analysis calculates the short-circuit current contribution for hypothetical fault types and pre-fault operation conditions to evaluate the possible impacts of a fault on the grid. Short-circuit analysis results can be used to verify the relay protection settings and operation, as well as the circuit breaker and fuse ratings, and to propose more accurate relay settings or a better feeder-circuit configuration from the viewpoint of circuit protection. Short-circuit calculations are also an integral step in determining the short-circuit ratio of a system, which is a measure of the strength of the system. The short-circuit ratio is used to identify areas that may impact system perturbations and system disturbances.

When a fault occurs in a distribution circuit, each DER connected to the circuit will contribute short-circuit current to the fault. The short-circuit analysis must include dynamic models of the DER generators in the calculations, especially for rotational-machine-based DERs. For inverter-based DERs, their individual short-circuit current contributions may be insignificant because the power electronic devices in the DERs can respond quickly to effectively limit the fault current contribution, which is 1.2–2.5 times normal current [8]. However, with large-scale penetration of inverter-based DERs, their fault current contributions must be considered. Normally, a current-limited Norton equivalent with control loops is required to adequately represent the short-circuit contribution from a DER.

2.2 DER MODELING IMPACT ON DYNAMIC STUDIES

This section mainly focuses on discussing the DER modeling impact on two types of dynamic studies, namely, disturbance ride-through analysis and transient stability analysis. The former is used to determine bulk system frequency and voltage stability following transmission faults with consideration of the amount of DER power that may be tripped off-line during the disturbance due to under-voltage, over-voltage, under-frequency, or over-frequency protection.

Transient stability analysis is employed to determine bulk system transient stability during and following transmission faults with consideration of a fast reactive power support from DERs that may improve the transient stability of directly connected synchronous generation.

Modeling of DER in dynamic BES studies requires a solid understanding of DER performance based on both interconnection requirements and technology-specific DER performance and control systems.

2.2.1 Interconnection Requirements

For power system stability studies, interconnection requirements of DERs determine the network fault response performance of individual DERs, depending on their commissioning period, connection level or size, and operating agreements between the DER operators/owners and power system operators. Interconnection requirements of DERs are evolving as the penetration level of DERs increases.

The original interconnection requirements, such as IEEE Std. 1547-2003 [9], Federal Energy Regulatory Commission's (FERC) SGIP/SGIA [10]–[11], and the former CA Rule 21 [12], are more focused on the protection and safety aspects of DERs and the distribution system. The original IEEE Std. 1547-2003 mandates that the DER unit be able to detect voltage/frequency deviations and trip within pre-specified time responses, and isolate itself within 2 s of the formation of an unintentional islanding. However, during a transmission contingency, the deviated voltage and/or frequency condition experienced throughout the entire grid may cause the DERs to trip, which may further reduce the total available generation and thus endanger the bulk power system stability. Similarly, momentary voltage sag caused by a fault on an adjacent feeder may cause DERs to trip. For these reasons, revisions of these standards are ongoing [13]–[16] to allow for the frequency/voltage ride-through capabilities of DERs, which take into consideration the stability and security of the BES.

Future revisions may bring additional dynamic performance requirements for DERs during and/or following network faults, similar to the requirements in Germany [17] for an additional reactive power injection to support voltage during faults.

2.2.2 Dynamic DER Models

Because of the complexity of DER dynamic behavior, when it comes to the modeling of DERs in dynamic BES planning studies, it may require a certain degree of simplification to limit the data and computational requirements. Model reduction could be achieved by one of the following or a combination of the two:

- Model aggregation (i.e., clustering of models with similar performance), and
- Derivation of equivalent models (i.e., reduced-order representation).

A dynamic equivalencing photovoltaic (PV) aggregation model, PVD1 [18], developed by the Western Electricity Coordinating Council (WECC), has been widely adopted. This model essentially lumps all the distributed DERs in the entire feeder or substation into one dynamic equivalencing model. It is not perfect because this approach, at best, gives an indication of the average response of the inverters which is not capable of capturing the individual PV inverter response, but it is considered the best in class [18]. As the technology and interconnection requirements evolve, PV system modeling will continue to evolve.

In general, the PVD1 model shall be suitable for studying system response to electrical disturbances, not solar irradiance transients. Electrical disturbances of interest are primarily balanced transmission grid faults (external to the solar PV power plant), typically 3–9 cycles in duration, and other major disturbances such as loss of generation or large blocks of load. Simulations performed using these models typically cover a 20- to 30-s time frame, with integration time steps in the range of 1 to 10 ms.

The capabilities and limitations of the PVD1 model are summarized as follows:

- The model assumes a fixed active power output and cannot incorporate emulation of irradiance changes in large-scale system dynamic studies.

- The model allows for certain active power controls, including over-frequency response with user-defined deadband and droop, ramp rate limits, etc.

- The model accommodates two basic reactive power control modes: constant reactive power and Volt-VAR control at the generator terminals. The Volt-VAR control is also referred to as Q-V control and the user can define Q-V characteristics in this control mode.

- The control actions that impact the behavior of the inverter during the short span after a fault are generally not modeled in detail. Therefore, the simplified model is not poised to evaluate the fault ride-through function of PV systems, i.e. determine whether the PV system would trip for a given voltage or frequency deviation for a period of time.

- Generation tripping: The model allows for tripping of all or a portion of the generation based on over- and under-voltage and frequency monitored at the equivalent generator terminals. The user can set the voltage and frequency deadbands, how much generation trips, and what fraction of the generation is restored as the disturbance subsides.

3 DEVELOPMENT OF A T&D COMBINED MODEL

The T&D combined model developed on the MATLAB/Simulink platform is elaborated in this chapter. The transmission system is a modified Kundur Two-Area network [19]. The distribution system modeled is a modified IEEE 34-node test feeder [20]. The T&D combined model can carry out static and dynamic simulations as well as electromagnetic transient (EMT) simulations. The distribution feeders modeled include single-phase and two-phase laterals. Three-phase as well as single-phase DER models were developed and integrated into the distribution network. These features will empower grid operators to accurately evaluate the aggregate effects of the unbalanced multi-phase DERs on the T-D interface. This T&D combined model will be used to examine DER impact on voltage stability, frequency regulation, and dynamic stability of the BES in later chapters.

The DER inverter modeling developed includes both detailed and average models. A detailed model of a DER inverter is done at the component level, so that the electromagnetic dynamics related to insulated gate bipolar transistor (IGBT) switching in inverters and DC/DC converters can be studied. The detailed DER inverter model can be used for any harmonics or transient studies in both distribution and transmission systems. In the case in which the electromagnetic transients of the IGBT switching are not of concern, an average dynamic model of the grid-connected inverter is used. The average model incorporates all the control and inverter response dynamics but excludes the switching dynamics and associated harmonics.

3.1 TRANSMISSION SYSTEM MODEL

The modified Kundur Two-Area system [19] was selected to faithfully represent all the operation modes and dynamics of a BES. The two area systems are connected by a 220-km long double transmission line. A schematic diagram of the modified Kundur Two-Area system is shown in Figure 1. The aggregated load model in each area is modified such that part of the original load centers are replaced by distribution feeders represented as DS. The distribution feeders are integrated with different DER components, as discussed in the next section. When DER penetration is increased in an area, the generation capacity and overall inertia in that area are scaled down accordingly to reflect the effect of DERs displacing conventional generators.

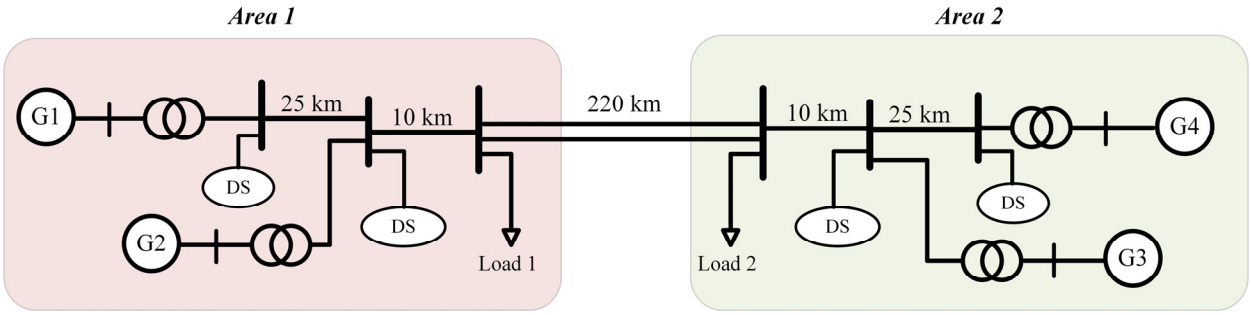

FIGURE 1 Schematic diagram of modified Kundur Two-Area system.

3.2 DISTRIBUTION SYSTEM MODEL

The distribution system modeled is the modified IEEE 34-node test feeder [20]. Both balanced and unbalanced feeder models were developed and will be discussed in this section.

3.2.1 Balanced Feeder Model

The balanced feeder model of the modified IEEE 34-node test system consists of a total of 22 symmetrical line segments. A schematic diagram of the balanced test feeder is shown in Figure 2. Characteristics of the designed test feeder are as follows:

- Maximum Feeder Capacity: 12.5 mega volt-ampere (MVA), Feeder Nominal Voltage: 12.47 kV L-L
- Nominal Load: 7.92 MW, 2.57 mega volt-ampere reactive (MVAR)
- Substation Transformer: 15.6 MVA, 230-kV D/12.47-kV Gr. Y, R = 1%, X = 8%
- Loads are assumed to be either spot or distributed. Spot loads are aggregated at a particular node in the feeder. Distributed loads are equally distributed on two nodes connected by a distribution line.
- Four capacitors are placed at various locations in the feeder to maintain voltage within acceptable limits.

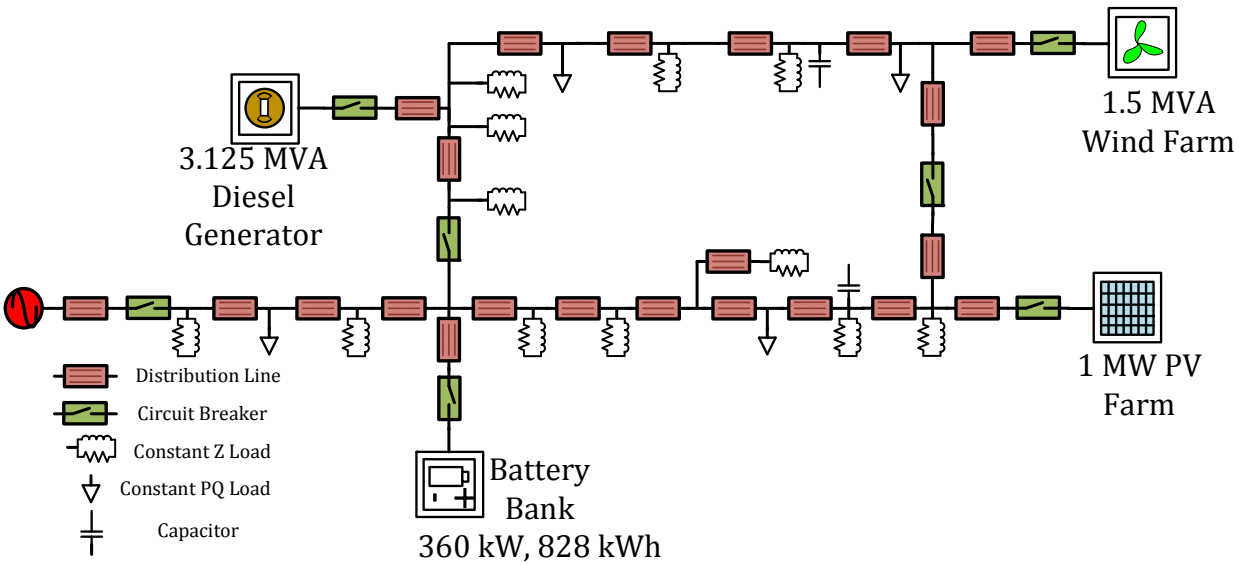

FIGURE 2 Schematic diagram of the modified IEEE 34-node test feeder.

Four different types of DERs were integrated into the distribution system model and will be discussed in the next section.

The connectivity, line segment configuration data, load data, and capacitor bank data can be found in Appendix A.

3.2.2 Unbalanced Feeder Model

The following changes were made to the balanced distribution system to create an unbalanced feeder model.

- Line configuration 603 of 0.5 miles was added with a load of 0.23 MW and 0.132 MVAR from Node 4.
- Line configuration 607 of 0.5 miles was added with a load of 0.128 MW and 0.086 MVAR from Node 4.
- Line configuration 303 of 0.5 miles was added with a load of 0.128 MW and 0.086 MVAR from Node 5.
- Line configuration 302 of 0.5 miles was added with a load of 0.128 MW and 0.086 MVAR from Node 621.
- Line configuration 302 of 0.5 miles was added with a load of 0.128 MW and 0.086 MVAR from Node 64.
- Line configuration 304 of 0.5 miles was added with a load of 0.128 MW and 0.086 MVAR from Node 7.
- Line configuration 604 of 0.5 miles was added with a load of 0.23 MW and 0.132 MVAR from Node 723.
- Line configuration 604 of 0.5 miles was added with a load of 0.23 MW and 0.132 MVAR from Node 77.

3.3 THREE-PHASE DER MODELING

Four different types of three-phase DERs are integrated into the distribution system model: PV farm, wind turbine generator (WTG), utility-scale battery energy storage system (BESS), and diesel generator. The portfolio of DERs modeled in the distribution system is shown in Figure 3.

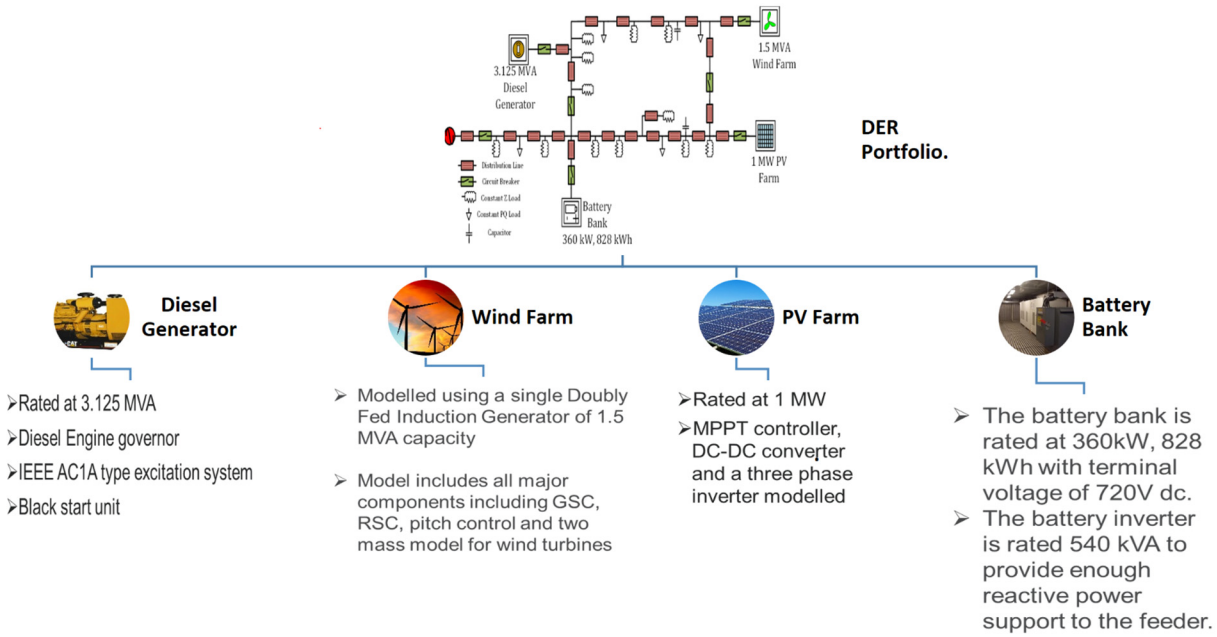

FIGURE 3 DER modeling portfolio in the test feeder.

The characteristics of the DER systems integrated into the test feeder are as follows:

1. The system has a provision to operate in both islanded and grid-connected modes.

2. The diesel generator can be used for black start.

3. The system is designed to operate in both radial system configuration and loop configuration.

4. DERs are connected to a distribution node via a transformer which has a rating equal to the VA rating of the DER.

5. Each DER has its own circuit breaker and protection logic scheme, which is implemented according to IEEE Std. 1547a-2014 [13], as shown in Table 1 and Table 2.

6. The DER systems modeled in totality include a detailed representation of DER inverters. The detailed model of the DER inverter entails individual component-level modeling. Individual component-level modeling is required so that the electromagnetic dynamics related to IGBT switching in the inverters and DC/DC converters can be studied. The detailed DER inverter model can be used to perform all harmonics and/or transient studies in both distribution and transmission systems.

7. In the case in which the electromagnetic transients of the IGBT switching are not of concern, an average dynamic model of the grid-connected inverter is used. The average model incorporates all the control and inverter response dynamics, but excludes the switching dynamics and associated harmonics.

8. The time step used for the simulation is 50 μs.

9. The battery inverter, PV inverter, and wind generator have the ability to operate in one of the following three modes of control:

    1. **Voltage control mode**: The DER system tries to maintain its point-of-common-coupling (PCC) voltage through adjusting its reactive power output following local Volt-VAR droop control. An exemplary Volt-VAR droop control curve is shown in Figure 4. The voltage reference points and the slope of the curves can be specified by the grid operator.

    2. **Reactive power control mode**: The DER system tracks the reactive power setpoint specified by the grid operator. The distribution system operator can perform load flow or state estimation in the distribution system, on the basis of which the operator can dispatch certain inverter-based DERs to provide reactive power support to the grid.

    3. **Power factor control mode**: The DER system tracks the power factor setpoint at the PCC determined by the grid operator. In this case, as the active power output of the DER system changes, the reactive power from the DER system also changes accordingly such that the overall power factor at the PCC is maintained constant.

10. DERs are also equipped with droop control for frequency regulation. This control mode is interchangeably referred to as P-F control. The droop control is implemented by using a proportional control that considers frequency deviation as the error and the corresponding change in power as control output.

TABLE 1 Interconnection System Response to Abnormal Voltages

Default Settings		Range of Adjustability
Voltage Range (% of Base Voltage)	Clearing Time (s)	Clearing Time (s): Adjustable Up To and Including
V < 45	0.16	0.16
45≤ V <60	1	11.00
60 < V< 88	2	21.00
110 < V< 120	1	13.00
V≥ 120	0.16	0.16

TABLE 2 Interconnection System Response to Abnormal Frequencies

	Default Settings		Ranges of Adjustability	
Function	Frequency (Hz)	Clearing Time (s)	Frequency (Hz)	Clearing Time (s): Adjustable Up To and Including
Under Frequency (UF) 1	< 57	0.16	56–60	10
Under Frequency (UF) 2	< 59.5	2	56–60	300
Over Frequency (OF) 1	> 60.5	2	60–64	300
Over Frequency (OF) 2	> 62	0.16	60–64	10

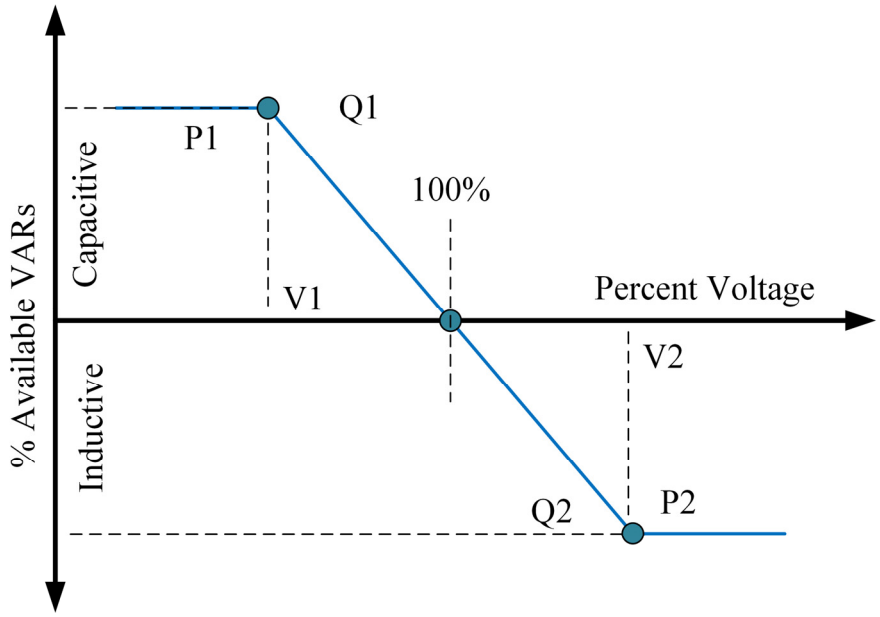

FIGURE 4 Representative inverter-based DER system Volt-VAR droop control curve.

The detailed configuration and operational parameters for each of the three-phase DERs can be found in the Appendix A.

3.4 SINGLE-PHASE DER MODELING

The single-phase DER system in the developed distribution system model consists of two types of renewable energy resources. The first one is based on a residential-scale single-phase PV system, and the other is a BESS, also designed for single-phase systems. Even though the generation sources of the DER systems differ, the controls of the inverter for both DER systems are similar. Two types of controls were implemented for single-phase DER systems: hysteresis-based control and DQ reference-frame-based control.

(a) Hysteresis-based control. The most basic way to model a grid-connected single-phase inverter is through a hysteresis current control loop. In this form of control, the current magnitude and current phase are computed based on the active and reactive power setpoint given to the inverter and the measured value of grid voltage. With the knowledge of the grid frequency, an instantaneous waveform is created for current reference. The current reference waveform is then compared to the measured current on an instantaneous basis. The current error is then compared directly to a hysteresis band using comparators to create the phase leg switching commands for the Voltage Source Converter [21]. For a residential PV system, the active power reference can be obtained from an irradiance profile, while for a BESS, a supervisory control loop based on ancillary service requirements can provide the active power reference. The reactive power reference for both the PV system and the BESS can be based on either (a) power factor control or (b) voltage regulation.

(b) DQ reference-frame-based control. In this control topology, the reference frame theory generally applied to three-phase systems is applied for controlling the bi-directional flow of active and reactive power of a single-phase inverter. The advantage of using this control topology as opposed to the hysteresis-based one is that the control variables become DC quantities, and a fixed switching frequency can be used for the inverter as opposed to a variable switching frequency for the hysteresis-based control [22].

The control schemes and configuration parameters for both hysteresis-based control and DQ reference-frame-based control developed for single-phase inverters are given in Appendix A.

3.5 INTEGRATED T&D COMBINED MODEL AND ITS KEY CAPABILITIES

The diagram of the integrated T&D combined model is shown in Figure 1. The key capabilities of this T&D combined model are as follows:

- Capability to model multi-phase DERs in distribution systems in order to understand the aggregate effects of the unbalanced multi-phase DERs on the T-D interface.

- Capability to carry out steady-state, dynamic, and electromagnetic-transient simulations.

- Flexibility to implement DER interconnection standards such as IEEE Std. 1547 on DER interconnection models. This flexibility can facilitate BES disturbance ride-through studies with expanded frequency and voltage ride-through ranges.

- Flexibility to implement advanced DER control functions such as Q-V and P-F control in order to help assess the potential for improving BES reliability by transforming DERs to an active “support reliability” resource.

In general, this T&D combined model is an effective analysis vehicle to understand the level of reliability impact of DERs on the BES and evaluate advanced control strategies to improve BES reliability. Specifically, the T&D combined model has value as an analytical tool for steady-state and dynamic analyses for planning purposes, and for operational studies. The model can be used for EMT studies as well.

Steady-state simulations will enable the following analyses:

- Short-term and long-term BES planning studies including power flow analysis, short-circuit analysis, and contingency analysis.
- BES voltage stability studies following small disturbances.

Dynamic simulations will reinforce the following analyses:

- BES voltage stability studies following large disturbances such as faults or loss of load or generator.
- Dynamic stability analysis including small-signal stability and transient stability.
- Frequency stability analysis including inertial frequency response, primary frequency response, and spinning reserve.
- Protection studies.
- Disturbance ride-through studies.

In conjunction with other operational software or application, the model can be used to carry out operational studies for BESs, including:

- Impact on the system's secondary frequency response, typically controlled through the system operator's AGC.
- Impact on the load following or ramping requirements throughout the day and over the course of the seasons through economic dispatch.

EMT simulations can support the following studies:

- Harmonic studies for power quality related issues.
- DER switching transient induced issues.
- Validation of protection applications such as fault location and reclosing algorithms.

4 SURVEY OF REAL-TIME FREQUENCY ESTIMATION AND PREDICTION TECHNIQUES

Power system frequency is an important parameter in identifying an abnormal behavior in the power system. Following a disturbance, the system frequency changes with time and may lead to system failure if appropriate corrective measures are not taken. This risk necessitates a frequency estimation method that will not only adaptively estimate the system frequency, but also predict its future behavior. In principle, the frequency can be derived efficiently from voltage and current signals if they are pure sinusoids; however, owing to the complex nature of a power system that contains multiple time-varying components and includes harmonic content, the measured waveforms are distorted. As a result, the frequency estimation method requires a more accurate time-varying system model that incorporates the system and measurement uncertainty.

In this chapter, the findings from a literature survey on various real-time frequency estimation and prediction techniques for sudden changes in system frequency due to intermittent DERs are presented, along with appropriate actions to provide frequency support.

4.1 BACKGROUND

The intermittent behavior of DERs may result in deviation of the system operating condition from its nominal value randomly and frequently. The random change in system operating condition can be reflected in terms of frequency deviation. If this frequency deviation exceeds the specified value, it may have a detrimental impact on system reliability and stability. Thus, in order to take corrective action, it is essential to know the system frequency in real time. Conventional generation resources include frequency-sensing equipment, or governors, that automatically adjust electricity output within seconds in response to frequency to correct out-of-balance conditions. This feature is restricted in a system with high penetration of renewables, mainly because (a) a high penetration of DERs reduces the system inertia, which in turn restricts the initial frequency response to arrest frequency decline and stabilize the system frequency following a contingency, and (b) most of the DERs operate at their maximum power and there is limited or no scope for them to adjust their power output so that they could participate in primary frequency response. To overcome this issue, it is essential for DERs to participate in frequency response. This outcome can be achieved through modeling the DERs with virtual inertia characteristics and adjusting the control setting of the DERs, allowing them to participate in frequency response. The knowledge of system frequency in real time is key. One way to obtain this knowledge is to deploy a large number of frequency-sensing devices and communicate the frequency information to controllers. However, this solution is economically infeasible. Thus, frequency estimation and prediction techniques that utilize available voltage and current measurements to estimate/predict the frequency in real time need to be included in the controller. The rapid change in DER output warrants a fast frequency estimation technique.

4.2 CHALLENGES IN FREQUENCY ESTIMATION

Accurate estimation of the power system frequency in real time is a prerequisite for rapid-response applications, including load shedding, generator protection, and renewable-energy control. In addition, the outcome of the frequency estimation technique is highly impacted by parameter uncertainty. Thus, the frequency estimation method should address the following challenges:

1. ***Speed***: Real-time applications require fast frequency estimation. The estimation should converge rapidly.

2. ***Accuracy***: The frequency estimation method should accurately track the frequency irrespective of rapid changes in system operating conditions.

3. ***Parameter uncertainty***: The method should account for steady-state and dynamic changes in system parameters and parameter uncertainty.

4.3 FREQUENCY ESTIMATION METHODS

Several techniques for frequency estimation are described in the literature. The predominant methods can be broadly classified into seven categories:

1. *Zero-crossing/modified zero-crossing methods [23]–[24]*
   The zero-crossing method estimates the frequency by measuring the time interval between two consecutive zero crossings of a signal. Although the method is simple, it may fail to produce the correct results because of harmonic distortion of the signals, presence of local zero crossings, signal processing round-off errors, and signal noise. The method is particularly useful in steady-state frequency estimation. The intermittent behavior of DERs results in dynamic changes in power system frequency; thus, this method is not suitable for frequency estimation in a power system with high DER penetration. Another issue with this method is slow speed of convergence.

2. *Discrete Fourier Transform [25]–[27]*
   The Discrete Fourier Transform (DFT)-based method for frequency estimation is a classical technique that estimates the frequency from the time variation of the signal sequence obtained from the DFT coefficient of the positive fundamental frequency. The main drawback of this method is that the discrete nature of FFT results in large estimation errors. One of the proposed methods to eliminate these errors is to use interpolation. The interpolation-based DFT method extracts the frequency information from the signal by means of interpolation and requires the use of multiple samples of the DFT spectrum. Other issues associated with DFT-based algorithms can cause frequency errors, mainly due to noise and the leakage effect of the negative

fundamental frequency[1] [28]. Many techniques have been proposed to tackle this problem. Use of an adaptive sampling window and analytical methods have been proposed to cancel the error [29]-[30].

3. *Orthogonal techniques [24]–[27], [31]–[33]*
   In orthogonal methods, the signal is decomposed into its orthogonal components and the frequency information is obtained from the decomposed signal. Typically, the input signal is digitized and sampled at a pre-specified sampling rate (at least twice the fundamental frequency) and a finite impulse response filter derived from the DFT of the signal is designed to orthogonalize the signal. Although this technique is suitable for real-time fast frequency estimation, the accuracy of the estimation is impacted by filter gains. The filter gains of orthogonal components drift the frequency from its nominal value. One way to overcome this problem is to use adaptive filtering [34] and to rely on historical sample information [35].

4. *Least squares [36]–[38]*
   This method works by minimizing the square of the error between observations and estimates obtained from mathematical models governing the observations, which include frequency. Thus, the outcome of this method provides an estimate of frequency. Typically, an observation is a nonlinear function of frequency; the algorithm estimates the frequency recursively. The advantage of this algorithm is high accuracy, but slow speed of convergence is a main drawback for real-time implementation.

5. *Kalman filtering/adaptive filtering [39]–[40]*
   The Kalman filter (KF) is a linear estimator that utilizes the system dynamics model and a series of measurements to estimate the system frequency. The method accurately estimates the frequency even when the signal is corrupted by noise and contains harmonics, provided that

   (a) The model used in the estimation accurately captures the system dynamics, and
   (b) System operating conditions do not change significantly.

   As per condition (a), the model should include the system uncertainties. If parameter uncertainties are not captured, the algorithm may yield wrong results. Similarly, condition (b) must also be met to ensure that the model can be linearized around an operating condition, given that the power system model is highly nonlinear. Condition (b) ensures that the behavior of the nonlinear model does not change significantly and the model can be approximated with a linear equivalence. This is true mainly because the KF is a linear filter and operates on a linear model representation of the system.

[1] The leakage effect can result when the sampling frequency is not an integer multiple of the fundamental frequency.

The main drawback of this approach is slow convergence due to successive linearization. To overcome this issue, other variations of KF such as the Extended Kalman Filter (EKF) or particle filters that take nonlinearity into account can also be used for accurate and fast frequency estimation.

It should be noted that in the presence of renewables, it may be difficult to meet conditions (a) and (b); thus, an adaptive filtering technique can be utilized.

6. *Newton-based methods [41]–[44]*
   In Newton-based methods, the frequency is estimated by minimizing the error between the estimations and the observations in a least-square sense. The problem is first formulated as an optimization problem and then solved iteratively through a Newton-based method, which is similar to that used in power-flow analysis. This method is based on the assumption that measurements are sinusoidal. The presence of harmonics and noise can cause error in frequency estimation with this method, necessitating that the system be observable after eliminating the erroneous measurements[2]. One of the main drawbacks of the Newton-based method is that it involves extensive computation and is limited to fundamental components of measurements.

7. *Neural network [45]–[46]*
   A neural network method can work with measurements containing harmonics or in cases where measurements contain incomplete information, or the number of measurements are limited to ensure the observability. The method involves extensive training of the neural network before it can be used for real-time estimation of frequency, but after the training the method is fast enough for real-time implementation.

The preferred method should be fast, accurate, and capable of handling parameter uncertainties. Given the complex nature of power system dynamics due to the presence of high DER penetration, the system can have a high degree of uncertainty. Thus, whatever algorithms are chosen for frequency estimation, they should adopt a model on the basis of system identification.

A significant component of various frequency estimation techniques is the availability of reliable data. A lack of good-quality data is a drawback in obtaining a good estimate of frequency for various monitoring and control applications. The FNET [47] system is an effort to create an extremely low-cost and quickly deployable wide-area frequency measurement system with high dynamic accuracy and requiring a minimal installation cost. The FNET system consists of multiple fault disturbance recorders, which form a sensor network and communicate high-precision voltage magnitude, angle, and frequency information to a centralized server. All the measurements are time-synchronized via the Global Positioning System. Measurements are

[2] A system is observable if the frequency can be uniquely estimated from an available set of independent measurements.

stored and managed in a database (an information management system). This data can be used for estimation and prediction of frequency by different methods.

4.4 SYSTEM IDENTIFICATION

Frequency estimation techniques are highly dependent on system models. The overall dynamics of the power system, which includes generator, network, and load dynamics, are very complex and nonlinear, with uncertainty in system parameters. To overcome the problem of parameter uncertainty or missing parameters (due to, e.g., brownfield installation), we need to develop system identification algorithms to identify the system model on the basis of measurements, and then apply the estimation technique to the identified model to estimate and predict the system frequency. The nonlinearity can be taken care of either by sequential linearization or by adopting nonlinear identification and estimation methods.

In the identification process, the model outputs are compared with system outputs of the same input signals. If the difference is within a satisfactory range, the identification phase is successful; if not, the procedure is repeated, re-adjusting the model parameters, until good behavior is observed. The system identification process is delineated in Figure 5.

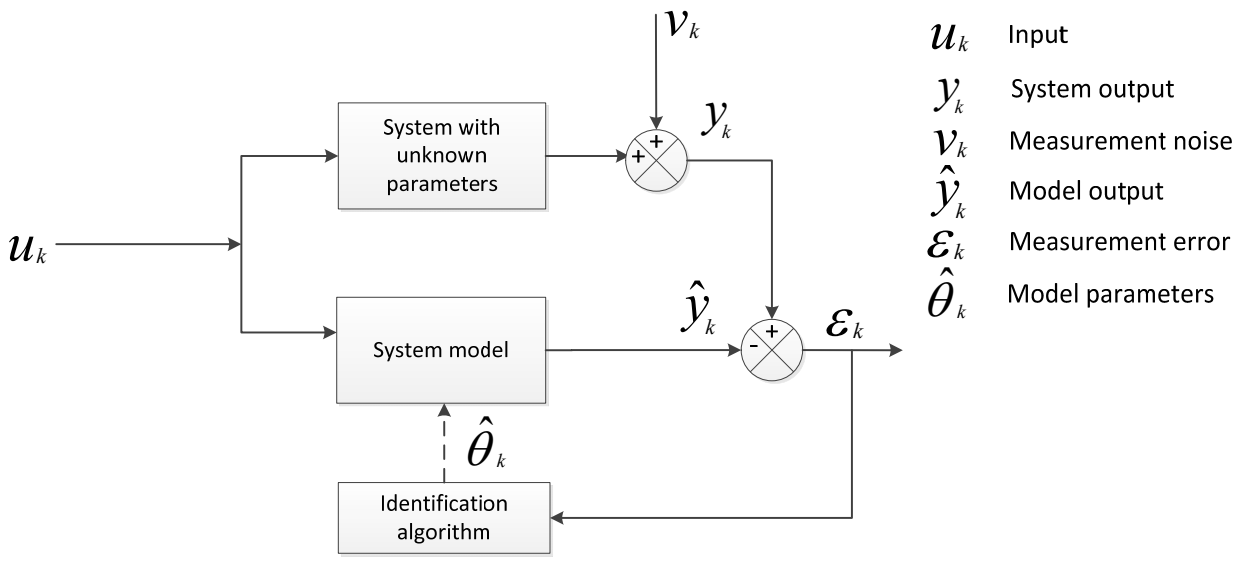

FIGURE 5 System identification process.

In the identification process, the system model can be a black-box, white-box or gray-box model. This process includes time series analysis and nonlinear system dynamics of the system. Regarding the identification algorithm, various heuristic and analytical methods can be explored. Alternatives include the following:

1. Least square
2. Maximum likelihood
3. Expectation-Maximization (EM) algorithm
4. Kalman filtering
5. Intelligent algorithm (Genetic Algorithm, PSO, ANN-based)

It is important to note that the system can be uniquely identified if there are adequate measurements. The measurements and their respective communication rates will be key in determining the identifiability of the system.

4.5 FREQUENCY ESTIMATION/PREDICTION

The linearized model obtained in the identification process can be represented in state space form as follows

$$\Delta\dot{\boldsymbol{x}}(t) = \boldsymbol{A}\Delta\boldsymbol{x}(t) + \boldsymbol{B}\Delta\boldsymbol{u}(t)+w$$

$$\Delta\boldsymbol{y}(t) = \boldsymbol{H}\Delta\boldsymbol{x}(t)+v$$

Here, $\boldsymbol{x} \in \mathbb{R}^n, \boldsymbol{u} \in \mathbb{R}^p$ and $\boldsymbol{y} \in \mathbb{R}^q$ are the vectors of state variables, inputs, and outputs, respectively; $\boldsymbol{A} \in \mathbb{R}^{n\times n}$, $\boldsymbol{B} \in \mathbb{R}^{n\times p}$ and $\boldsymbol{H} \in \mathbb{R}^{q\times n}$ are the state space matrices for the linearized open-loop system; and w and v are the process noise and measurement noise, respectively. The noise components are assumed to be Gaussian with i.i.ds.

The model in the discrete domain can be expressed as

$$\boldsymbol{x}_{k+1} = \boldsymbol{A}\boldsymbol{x}_k + \boldsymbol{B}\boldsymbol{u}'_k + \boldsymbol{w}_k;$$

$$\boldsymbol{y}_k = \boldsymbol{C}\boldsymbol{x}_k + \boldsymbol{v}_k$$

where $\boldsymbol{w}_k = \boldsymbol{B}\boldsymbol{w}'_k$, $\boldsymbol{w}'_k \sim N(\boldsymbol{0}, \boldsymbol{Q})$ and $\boldsymbol{v}_k \sim N(\boldsymbol{0}, \boldsymbol{Q})$.

From this model, the frequency can be estimated using the KF algorithm by following the steps shown in Figure 6. Note that the update steps of KF involve prediction of frequency.

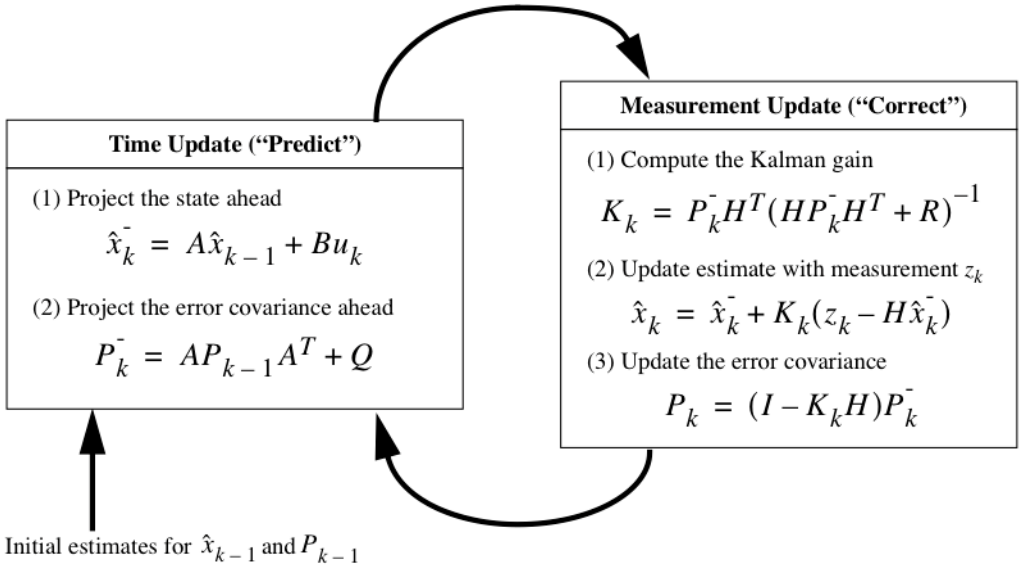

FIGURE 6 Frequency estimation using the Kalman Filter algorithm.

In addition to this method, the frequency can be estimated through a nonlinear model by using the EKF or the Unscented Kalman Filter, or directly by using the EM algorithm with KF. The latter approach to frequency estimation eliminates a separate identification stage.

The approach assumes that the distribution of measurement uncertainty is Gaussian. For a non-Gaussian scenario, we can adopt a Gaussian mixture model approach [48].

5 BENCHMARK CASE STUDIES

Using the MATLAB T&D combined model, six benchmark cases were studied to investigate the DERs' impact on the frequency regulation, voltage stability and dynamic stability of a BES. A diagram of the T&D combined model referenced throughout the case studies is shown in Figure 7.

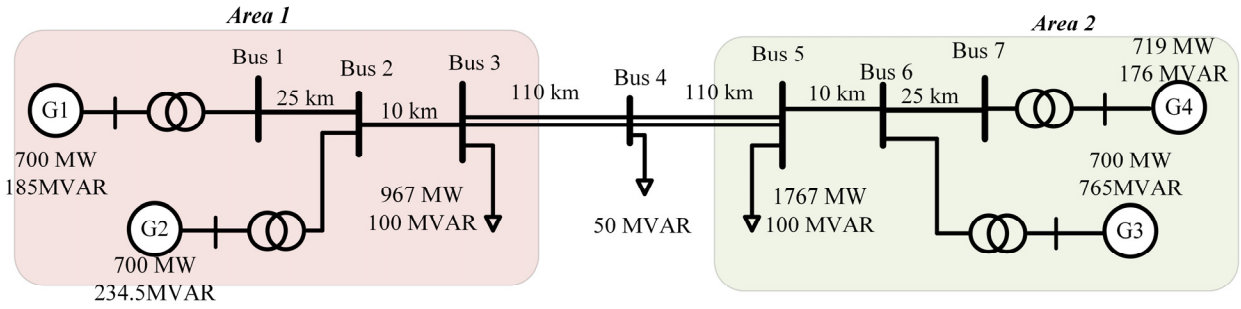

FIGURE 7 Diagram of the T&D combined model used for benchmark case studies.

5.1 IMPACT ANALYSIS OF DERs ON FREQUENCY REGULATION OF BES

In this section, the impact of DERs on BES frequency regulation, including inertial response, primary frequency response, AGC, and ramping/load following, is examined in three case studies. The results from each benchmark case are discussed below.

Case-FR-01: Effect of DERs replacing synchronous machines on inertial and primary frequency response of a BES

Inertial response is an inherent physical response of SGs that kicks in and adjusts electrical power output when there is an imbalance between generation and load. System frequency is considered to be constant when the rotor can sustain a constant speed, with a balance between mechanical power developed by the SGs and electrical power consumed by the load. However, in the event of a sudden loss of a large generator, for example, the total generation available in the system is reduced, but the load does not change instantaneously, causing an imbalance in the system. Responsibility for satisfying the load is automatically redistributed among the remaining online SGs. The extra electric power needed from each remaining generator is supplied by the rotational kinetic energy stored in the rotating mass of the generator shafts, which slows down the speed of the rotors and decreases the system frequency. The initial rate of system frequency decline depends on the total effective inertia of the entire electric power system, i.e., the higher the system inertia, the slower the initial rate of system frequency decline. Thus, the inertial response is not a form of automatic control, but rather a system inherent physical response.

The speed governing system of SGs is equipped with droop characteristics. Following a large system disturbance such as loss of load or generator, the SGs automatically adjust their output through speed governors to match the system load demand. This primary frequency response of SGs is in place to help arrest the system frequency deviation. Generators that have available headroom[3] and can respond immediately are qualified to provide primary frequency response.

In this case study, the AGC is disabled in order to isolate its influence and identify the effect of replacing synchronous machines with DERs on the inertial response and primary frequency response of a BES. In addition, DERs do not provide any emulated inertial response service in this case study.

The total synchronous capacity, total inertia, and total load in each area in the Kundur Two-Area system are displayed in Table 3. In the system, there are two aggregated SGs in each area, each rated at 900 MW. Each SG in Area 1 has an inertia of 6.5 s, and each SG in Area 2 has an inertia of 10 s. The total load in Area 1 is rated at 850 MW and the total load in Area 2 is rated at 1000 MW.

TABLE 3 Kundur Two-Area System Configurations for System Frequency Response Studies

	Total Synchronous Capacity (MW)	Total Inertia (s)	Total Load (MW)
Area 1	900*2	6.5*2	850
Area 2	900*2	10*2	1000

The total simulation time was 100 s, and a sudden load increase of 160 MW in Area 1 was introduced at 20 s. Four sets of simulations were conducted in which the DER penetration level in Area 2 was increased from 0 MW, to 100 MW, 400 MW, and finally 700 MW, accounting for 0%, 10%, 40%, and 70% DER penetration with respect to the total load in Area 2, respectively. For each DER penetration level, the SGs' capacity and inertia in Area 2 were reduced accordingly to simulate the effect of DERs displacing SGs and reducing total system inertia. Throughout all four sets of simulations, the configuration of Area 1 was kept constant, i.e., without any DER penetration.

Figure 8 delineates system frequency responses corresponding to different DER penetration levels. The horizontal axis denotes time, and the vertical axis represents the frequency deviation from 60 Hz measured at SG #3 in Area 2. The summary of various frequency response metrics measured at SG #3 are detailed in Table 4.

[3] Headroom refers to the available capacity for a generator to ramp up or down its electrical output.

The analysis results in Table 4 indicate that with decreased system inertia, the initial rate of change of frequency (ROCOF) is higher and the frequency nadir is lower after the load change. Another phenomenon observed is that with higher DER penetration, the settling frequency after the disturbance is lower. It can be concluded that when the DER penetration level increases in a BES, it is more challenging for the primary frequency control of the responsive SGs to arrest the frequency deviation after a disturbance. Therefore, reduced system inertia may threaten BES stability, and mitigation measures to compensate for lost inertia should be considered.

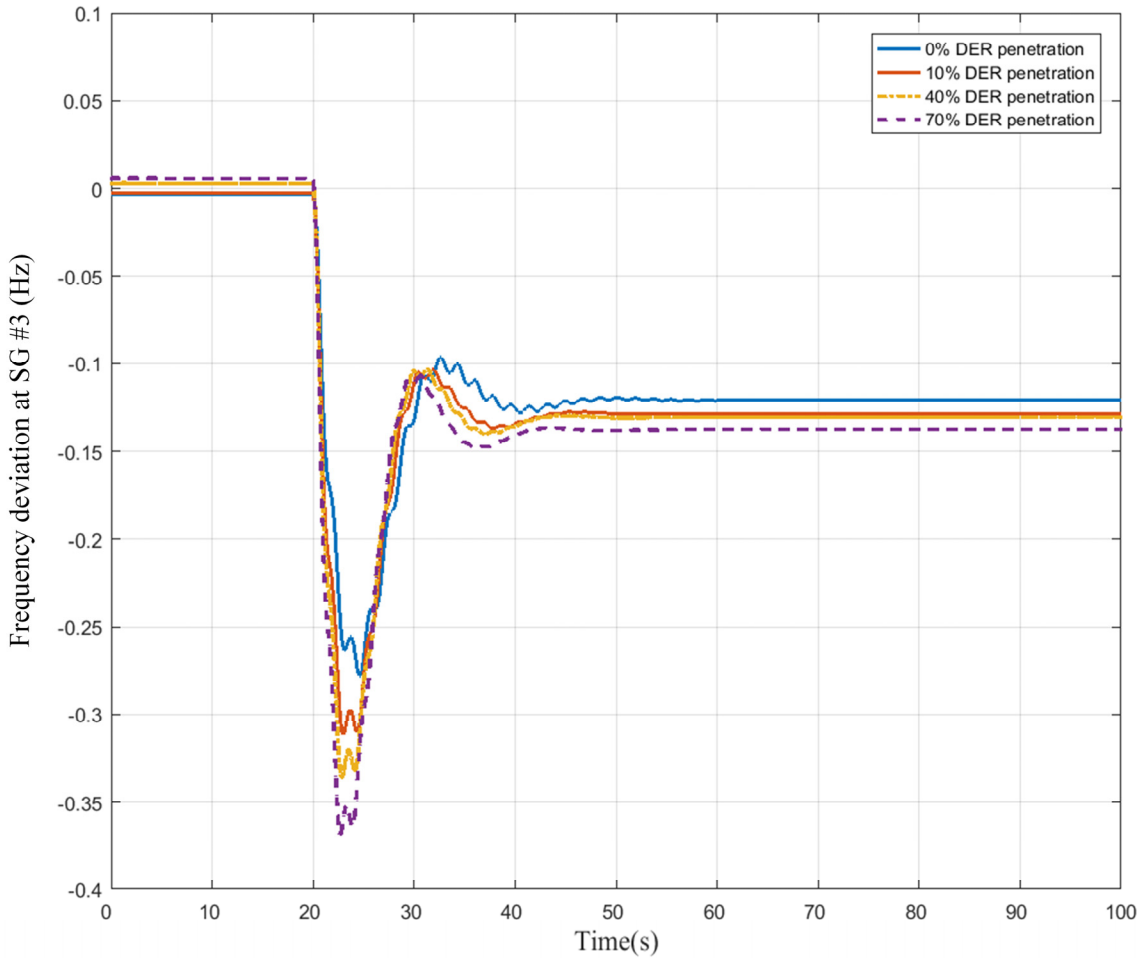

FIGURE 8 Effect of DER replacing synchronous machines and reducing system inertia.

TABLE 4 Summary of Various Frequency Response Metrics at SG#3 without AGC

DER Penetration Level	Frequency Nadir (Hz)	Initial ROCOF (Hz/s)	Settling Frequency (Hz)
0%	59.7243	0.058	59.8793
10%	59.6910	0.100	59.8714
40%	59.6649	0.118	59.8694
70%	59.6334	0.143	59.8625

Case-FR-02: Impact of DERs on AGC

AGC, sometimes called secondary frequency response, is another mechanism to restore the system frequency to its nominal value after a disturbance. The inertial response and primary frequency response controls can limit the initial rate of system frequency decline and arrest the frequency deviation, but the settling frequency of the system is unlikely to be at the nominal level. To fully restore system frequency, the grid operator applies AGC to increase or decrease the output of generators or loads that provide regulation services.

The AGC control used in the case study is shown in Figure 9. In order to remove residual error, a proportional-integral (PI) controller is used to generate the add-up value of the electrical power reference P_{ref} based on the rotor speed deviation Δω of the SGs. The integral term of the PI controller is limited so that it can react immediately in case of large changes in rotor speed ω (rad/s).

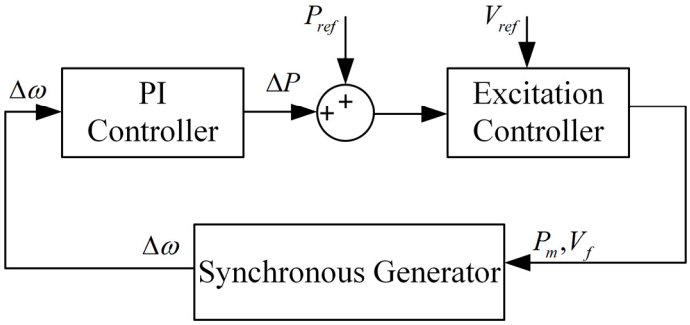

FIGURE 9 AGC implemented to study impact of DERs on AGC.

For this case study, the adopted system configuration, simulation conditions, and disturbance are the same as in the previous case, except that the AGC was enabled for all four sets of simulations. The frequency deviations at SG #3 in Area 2 corresponding to 0%, 10%, 40%, and 70% DER penetration level were plotted in Figure 10. The summary of various frequency response metrics measured at SG #3, including frequency oscillation and settling time,

are detailed in Table 5. Frequency oscillation in the table refers to the change in frequency magnitude from the nadir to the first spike after recovery.

It was observed from Figure 10 that as the DER penetration level increases, it takes longer for AGC to restore system frequency. The frequency restoration times for 0%, 10%, 40%, and 70% DER penetrations are 40 s, 45 s, 55 s, and 70 s, respectively. Larger and longer frequency oscillations upon the disturbance were also observed for higher DER penetration scenarios. The system's inability to quickly dampen these big swings could cause more equipment to trip off in order to protect itself, and thus possibly lead to a cascading failure.

Figure 11 compares the frequency deviation at SG#3 in Area 2 with and without AGC at 70% DER penetration level. It can be seen that with AGC, the system frequency eventually recovers to nominal value, which is 60 Hz in this case study. Without AGC, however, the system frequency settles at 59.8625 Hz, which is lower than the nominal value. This benchmark case study demonstrates that the AGC is a critical function to return system frequency to normal values after a disturbance, and it is more challenging for AGC to recovery system frequency with increased DER penetration levels.

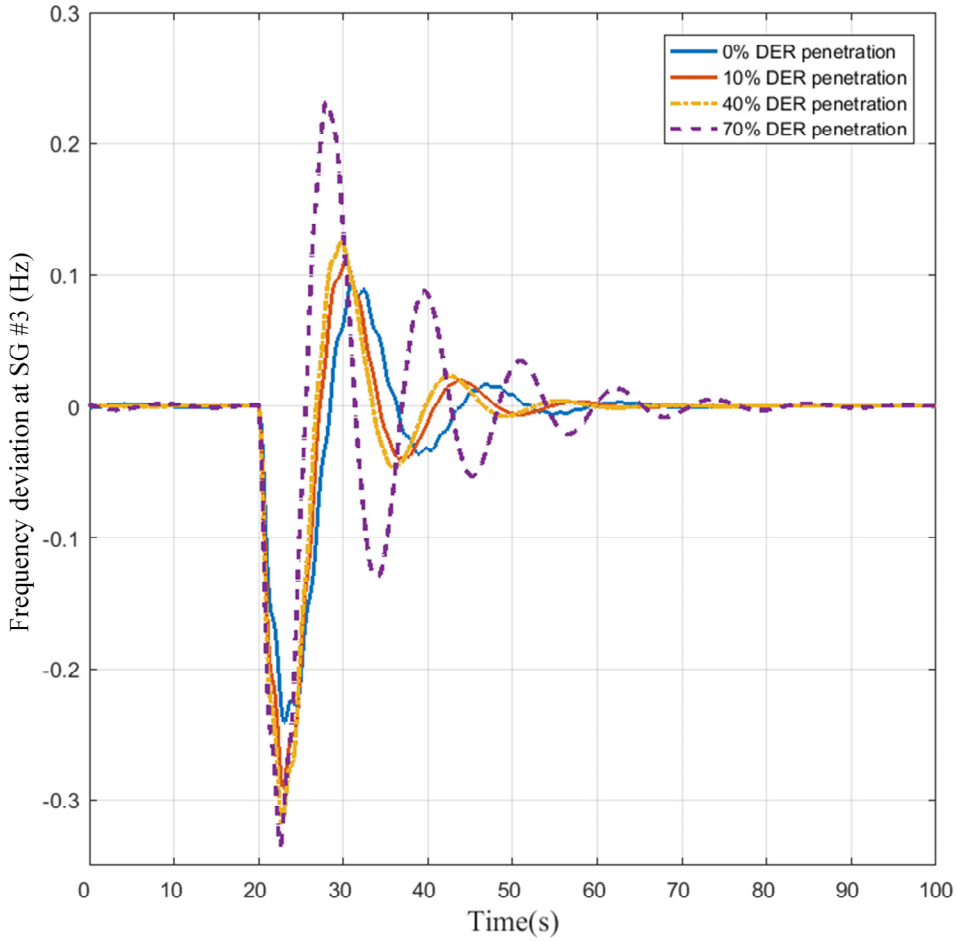

FIGURE 10 Impact of different levels of DER penetration on AGC.

TABLE 5 Summary of Various Frequency Response Metrics at SG#3 with AGC

DER Penetration Level	Frequency Oscillation (Hz)	Frequency Settling Time (s)
0%	0.3356	40
10%	0.4000	45
40%	0.4452	55
70%	0.5646	70

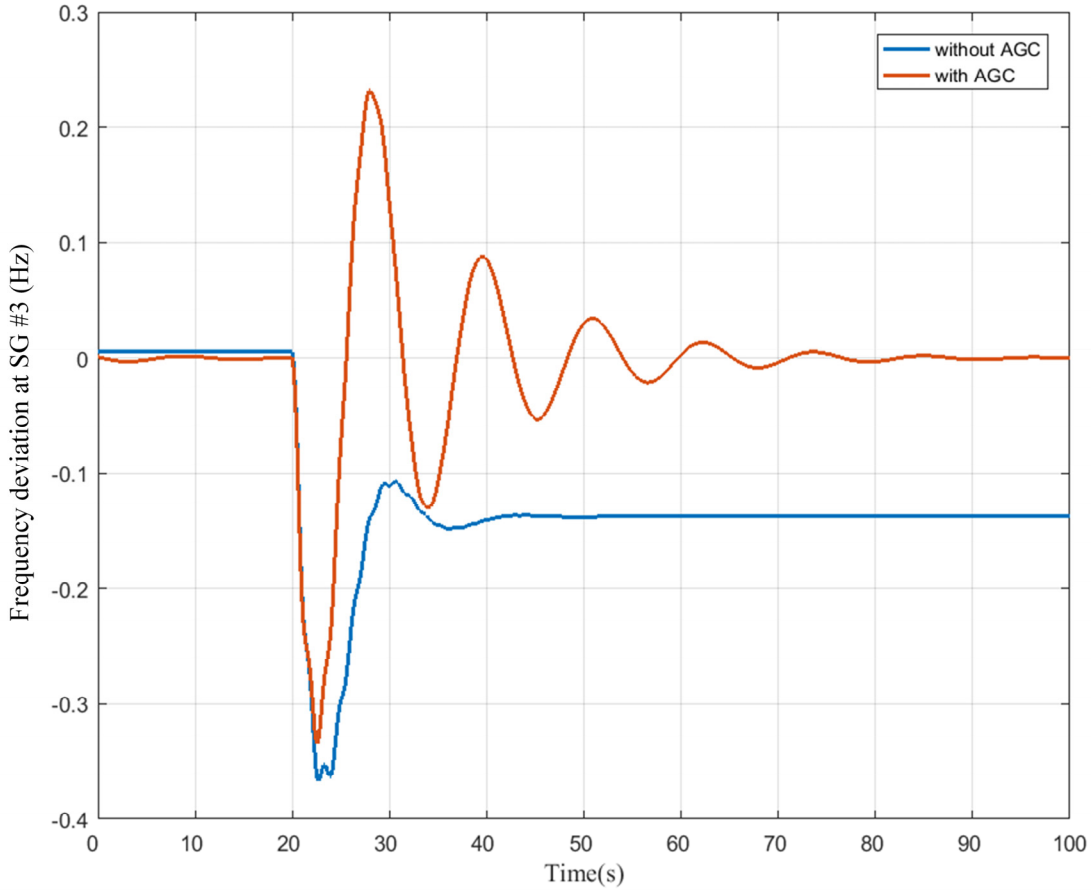

FIGURE 11 Comparison of system frequency responses with and without AGC.

Case-FR-03: Impact of DER on Load Following of a BES

In this case study, the Kundur Two-Area system was modified to model Bus 2 in Area 1 as the swing bus and Bus 3 in Area 1 and Bus 4 and 5 in Area 2 as the P-Q buses. A 24-hour load profile and PV profile were applied at Bus 5, shown in Table 6, to demonstrate the impact of PV penetration on BES load following. The load and PV profiles shown in Table 6 were scaled down by ten times from the original California Independent System Operator (CAISO) 2017

operational data[4] to fit the Kundur Two-Area system's original load setting. The values in Table 6 represent the scenario of 30% PV penetration compared to the load at Bus 5. The PV profile in Table 6 was then multiplied by 1/3, 2/3, 1, 4/3, and 5/3, respectively, while keeping the load profile as it is to create 10%, 20%, 30%, 40%, and 50% PV penetration scenarios.

The 24-hour real power injections at the swing bus are shown in Figure 12 for all five levels of PV penetration at Bus 5. Figure 12 exhibits a "duck curve" characteristic similar to that produced by CAISO. The three-hour ramping from 5 pm to 8 pm for all five PV penetration scenarios is shown in Table 7. Corresponding to 10% and 50% PV penetration levels, the three-hour BES ramping from 5 pm to 8 pm increased from 717 MW to 1424 MW, i.e., almost doubled. It is evident that as the PV penetration level increases, the challenges for BES load following increase as well.

TABLE 6 24-hr PV and Load Data at Bus 5

Hour	PV (MW)	Load (MW)
1	0	2295.072
2	0	2181.851
3	0	2105.728
4	0	2051.383
5	0	2026.752
6	0	2047.527
7	9.3	2095.343
8	223.8	2090.479
9	553.5	2008.627
10	710.5	1886.124
11	776.8	1865.933
12	837.4	1869.566
13	864.8	1869.274
14	861.1	1866.091
15	830.7	1909.262
16	641.7	2038.803
17	527.0	2297.685
18	348.8	2788.036
19	115.6	2870.095
20	2.6	2819.971
21	0	2757.098
22	0	2645.172
23	0	2467.232
24	0	2272.295

[4] http://www.caiso.com/market/Pages/ReportsBulletins/DailyRenewablesWatch.aspx#curtailment;

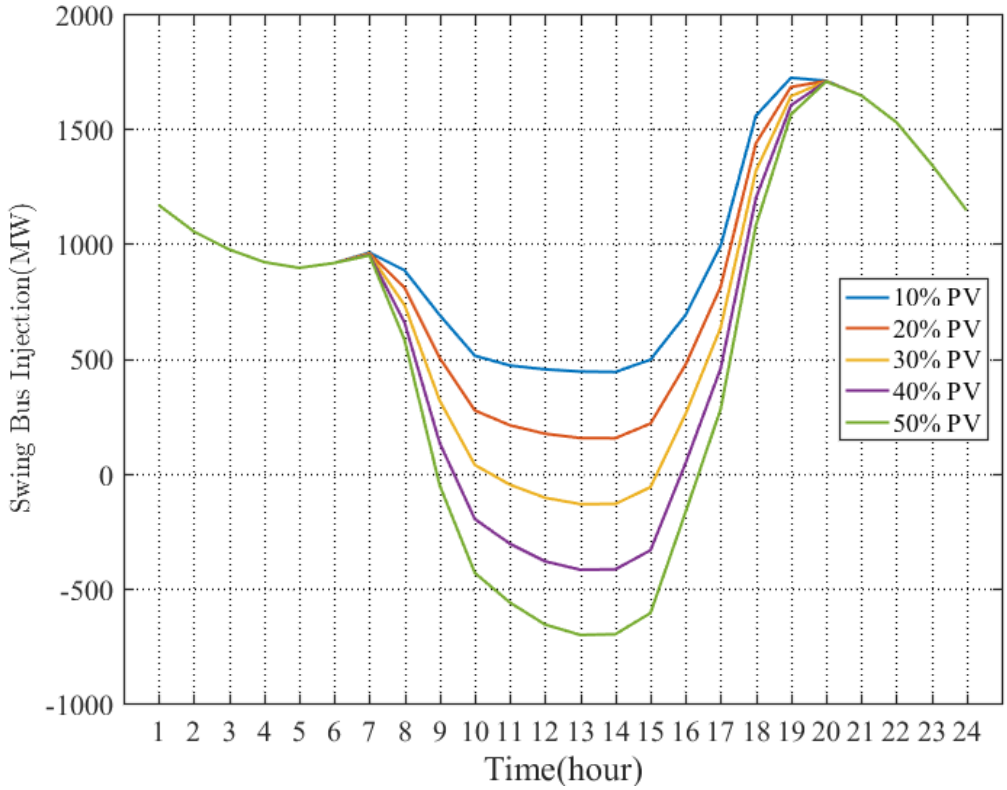

FIGURE 12 Impact of DER on BES load following.

TABLE 7 Three-Hour BES Ramping for Different PV Penetration Scenarios

PV Penetration Level	10%	20%	30%	40%	50%
3-hour (5 pm to 8 pm) BES Ramping (MW)	717.3	895.1	1072.3	1248.7	1424.4

5.2 DER IMPACT ON VOLTAGE STABILITY OF BES

In this section, the impact of DER on the voltage stability of a BES is investigated through one benchmark case study.

Case-VC-01: Effect of Intermittent DER Output on System Voltages and Frequency

The objective of this case study is to examine the impact of sudden change or intermittency of renewable energy resources on the system voltages and frequency. The total synchronous capacity, total inertia, and total load in each area in the Kundur Two-Area system are displayed in Table 8. DER is modeled as a battery storage system rated at 2.5 MW. The distribution feeder containing the DER is connected to Bus 5 in Area 2.

TABLE 8 Kundur Two-Area System Configurations for Voltage Stability Studies

	Total Synchronous Capacity (MW)	Total Inertia (s)	Total Load (MW)
Area 1	900*2	6.5*2	967
Area 2	900*2	6.175*2	1767

A battery power output oscillation with a frequency of 0.5 Hz was introduced at 20 s, changing from 2.5 MW positive (charging) to 2.5 MW negative (discharging) to simulate intermittent DER output. The low-frequency oscillation event is shown in Figure 13. The total simulation time was 50 s.

A collage of four subplots is shown in Figure 14. The first subplot depicts the relative machine rotor angle at SG 1, 2, and 3 with respect to the machine rotor angle at SG 4 throughout the entire event. The remaining subplots delineate the rotor speed, acceleration power of the power system stabilizer (PSS), and stator voltage at all four SGs throughout the entire event. All of these quantities are observed to experience the same sustained low-frequency oscillation at a frequency of 0.5 Hz. These low-frequency oscillations do not cause the DER protection system (such as IEEE Std. 1547 abnormal voltage/frequency deviations) to trigger, and they are not damped by PSSs. This is particularly undesirable, because once a contingency (e.g., loss of load or generation or a fault) occurs, the background low-frequency oscillations may amplify and possibly cause the entire system to collapse.

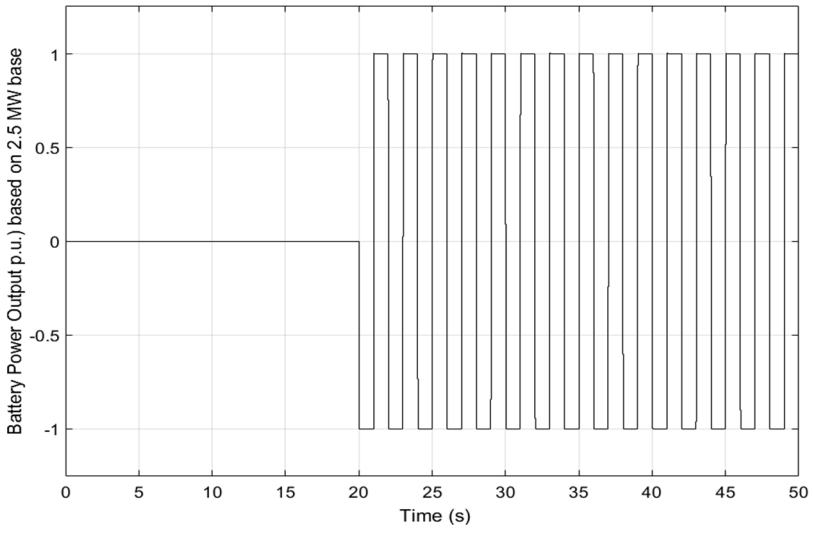

FIGURE 13 The event simulating intermittent DER output.

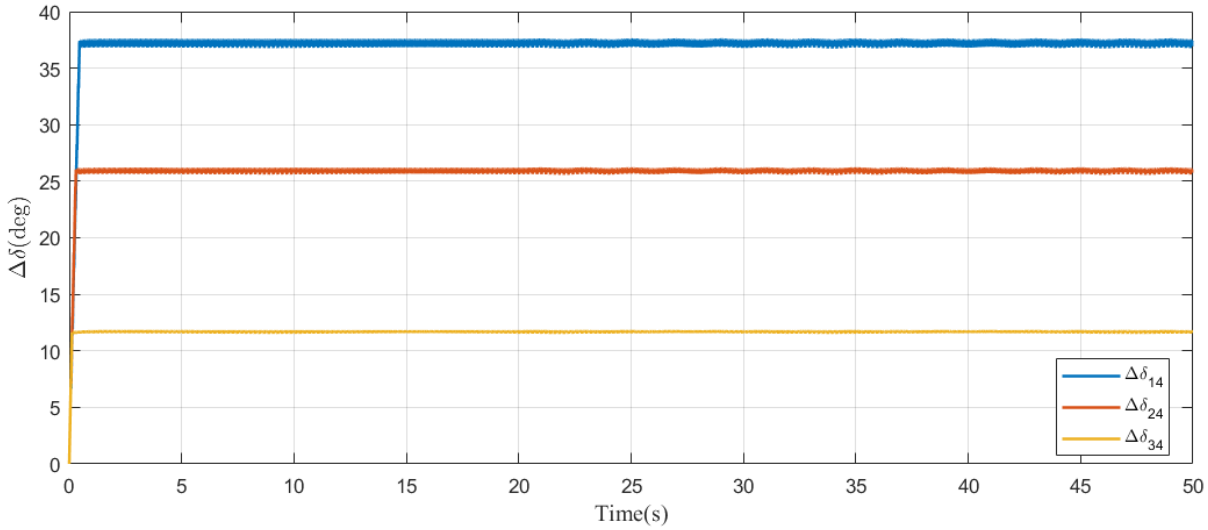
Δδ(deg)
Time(s)
Δδ14
Δδ24
Δδ34

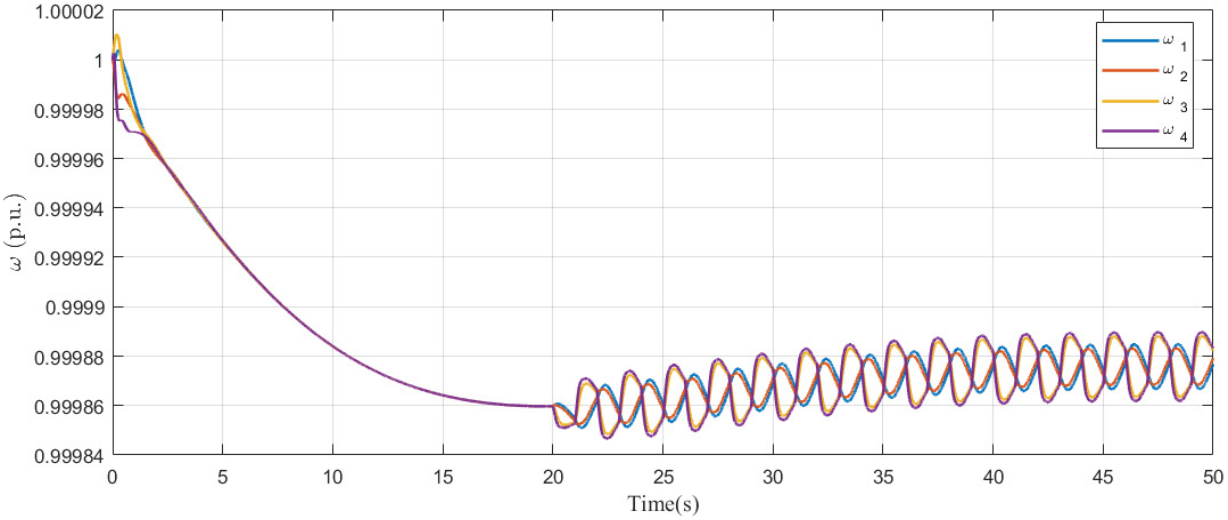
ω (p.u.)
Time(s)
ω 1
ω 2
ω 3
ω 4

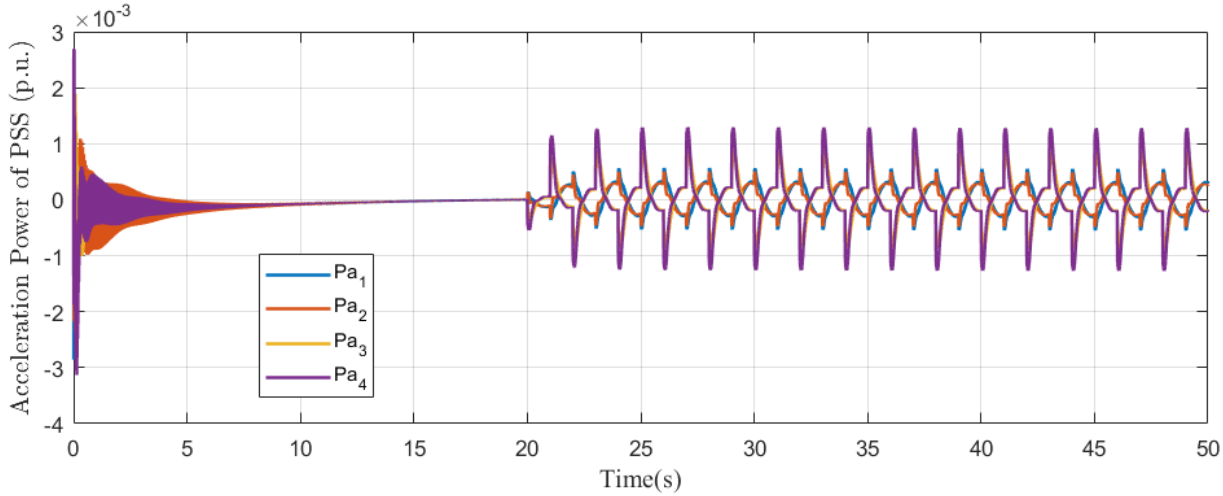
×10-3
Accelecration Power of PSS (p.u.)
Time(s)
Pa1
Pa2
Pa3
Pa4

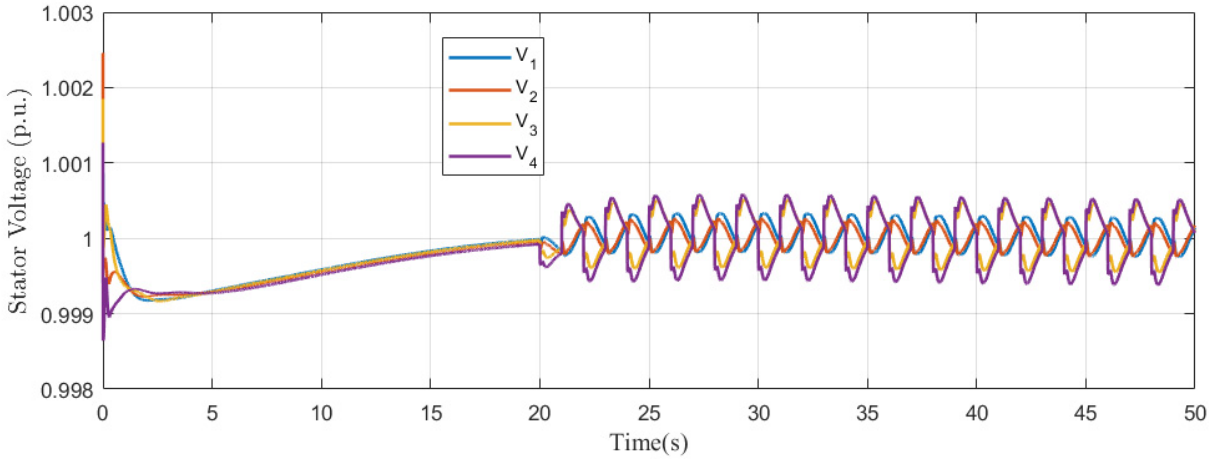

FIGURE 14 Effect of intermittent DER output on system voltages and frequency.

5.3 DER IMPACT ON DYNAMIC STABILITY OF BES

In this section, the impact of DERs on BES small-signal stability and transient stability is examined through two benchmark case studies using the T&D combined model.

Case-DS-01: DER Impact on the Small-signal Stability of a BES

The purpose of this case study is to illustrate the impact of DER integration on the small-signal stability of the BES. The linear state-space approach was used to describe the BES integrated with DERs, which is a complex nonlinear system. The DERs are connected in Area 2. Three operating scenarios corresponding to 0%, 13% and 30% DER penetration as compared to total load in Area 2 were considered, and are shown in Table 9. The linear analysis was performed on the two-area system model for each operating condition and corresponding eigenvalues were obtained from the system state-space matrix. Figure 15 shows the eigenvalue plot corresponding to the three levels of DER penetration. The direction of pole movement is indicated by the arrows in Figure 15. It is evident from the plot that when there are no DERs, the system poles all lie in the left half of the *s*-plane, indicating the system to be small-signal stable. As the penetration of DERs increases, the poles move towards the right half of the *s*-plane and eventually make the system small-signal unstable.

TABLE 9 Operating Scenarios for Various DER Penetration Levels in Area 2

DER Penetration Level	SG Capacity (MW)	Total Inertia (s)	Total Load (MW)	Total DER Output Power (MW)
0%	900*2	16.1*2	750	0
13%	600*2	6.175*2	750	97.5
30%	300*2	2.175*2	750	227.5

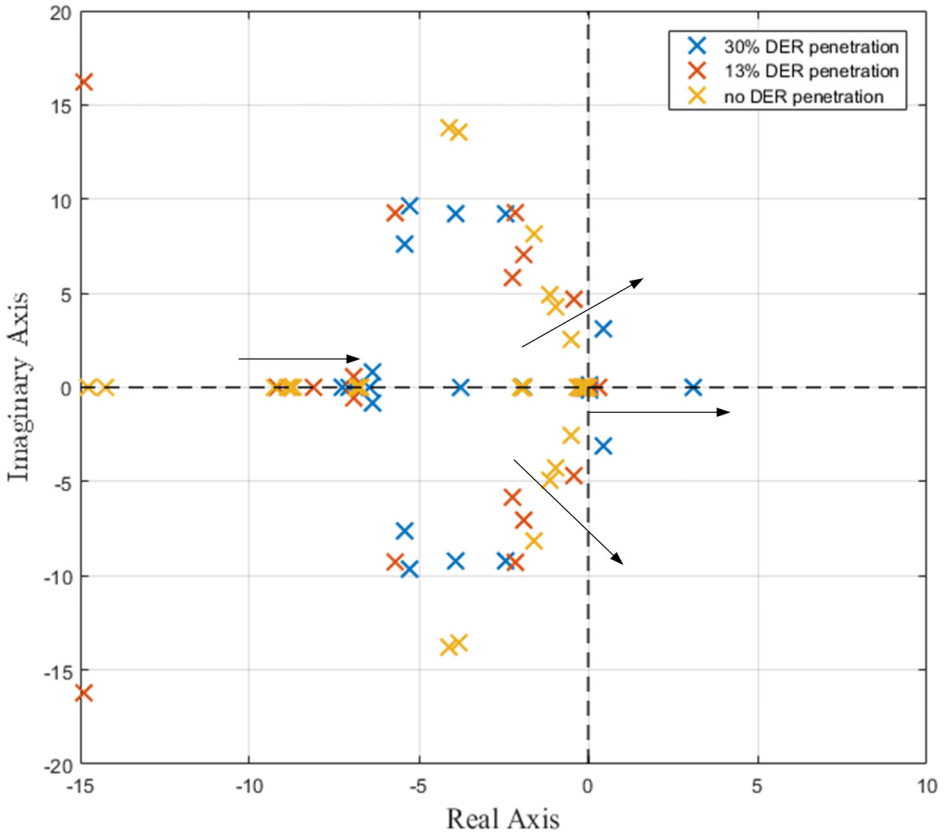

FIGURE 15 DER impact on small-signal stability of BES.

Case-DS-02: DER Impact on the Transient Stability of a BES

To study the impact of DERs on the transient stability of a BES, four scenarios were created. The first one was the base case without any DER penetration. Three levels of DER penetration, 16%, 33%, and 49%, connected at Bus 2 in Area 1, were then studied. The base-case total synchronous capacity, total inertia, and total load in each area in the Kundur Two-Area system are displayed in Table 10. It is noteworthy that all the DER systems are designed to operate in P-Q mode, where Q is set at 0 throughout the entire case study.

After 1 s into the simulation, a three-phase-to-ground fault with zero impedance was applied at 44 km from Bus 3 on one of the tie lines. The fault was cleared 12 cycles after the

TABLE 10 Kundur Two-Area System Configurations for Transient Stability Studies

	Total Synchronous Capacity (MW)	Total Inertia (s)	Total Load (MW)
Area 1	900*2	6.5*2	967
Area 2	900*2	6.175*2	1767

fault inception by circuit protection relays, placing the faulted tie line out of service. The total simulation length was 16 s. The DER response to abnormal frequencies and voltages based on IEEE Std. 1547a-2014 shown in Table 11 were implemented in the DER systems.

TABLE 11 Implemented DER Abnormal Voltage/Frequency Response[5]

Voltage Protection Settings		Range of Adjustability	
Voltage Range (% of Base Voltage)	Clearing Time (s)	Frequency (Hz)	Clearing Time (s)
V < 45	0.16	< 57	0.16
45≤ V <60	1	< 59.5	2
60 < V< 88	2	> 60.5	2
110 < V< 120	1	> 62	0.16
V≥ 120	0.16		

For each scenario, the same analysis was repeated with varying levels of DER penetration. The system responses, including tie-line two-terminal voltages and power flow, DER active and reactive power, DER trigger signal, and frequency and voltage at the DER PCC were plotted. In terms of the DER trigger signal, value 1 indicates that the DERs stay connected and value 0 indicates that the DERs are tripped off because of either abnormal voltage or abnormal frequency. The transmission-line-fault-induced phenomena during and after the fault are discussed below.

The system responses upon a transmission fault for 0%, 16%, 33% and 49% DER penetration scenarios are reported in Table 12. For higher DER-penetration scenarios, higher peak-to-peak oscillation value, faster DER tripping, and a longer time for the system to return to normal are observed. In conclusion, more DER penetration may put the power grid at risk of instability after a severe transmission system fault.

The base case without any DER penetration was first established and the tie-line voltages, tie-line power flow, and DER active and reactive powers throughout the entire event were plotted in Figure 16. Without any DER penetration, the voltages at two terminals of the tie line experienced a sag upon the fault occurrence and recovered after the protection devices cleared the fault and tripped the faulted line off. Tie-line power flow also quickly returned to its normal value after experiencing some spikes during the fault. The entire system was stable throughout the entire disturbance.

[5] The values shown in the table are a subset of complete IEEE Std. 1547a-2014.

TABLE 12 Summary of System Reponses Following a Transmission Line Fault for Various DER Penetration Scenarios

DER Penetration Level	DER Output Active Power (MW)	Tie-line Power Flow (MW)	IEEE Std. 1547 Protection Triggered?	Triggering Protection Mechanism	Triggering Time (s)	Oscillation Peak-to-Peak Value (MW)	Time Taken for System to Return to Normal (s)
0%	0	320	N/A	N/A	N/A	N/A	2
16%	155	420	No	N/A	N/A	N/A	4.1
33%	315	520	Yes	Overvoltage	2.35	850	14
49%	475	620	Yes	Overvoltage	2.01	990	>15

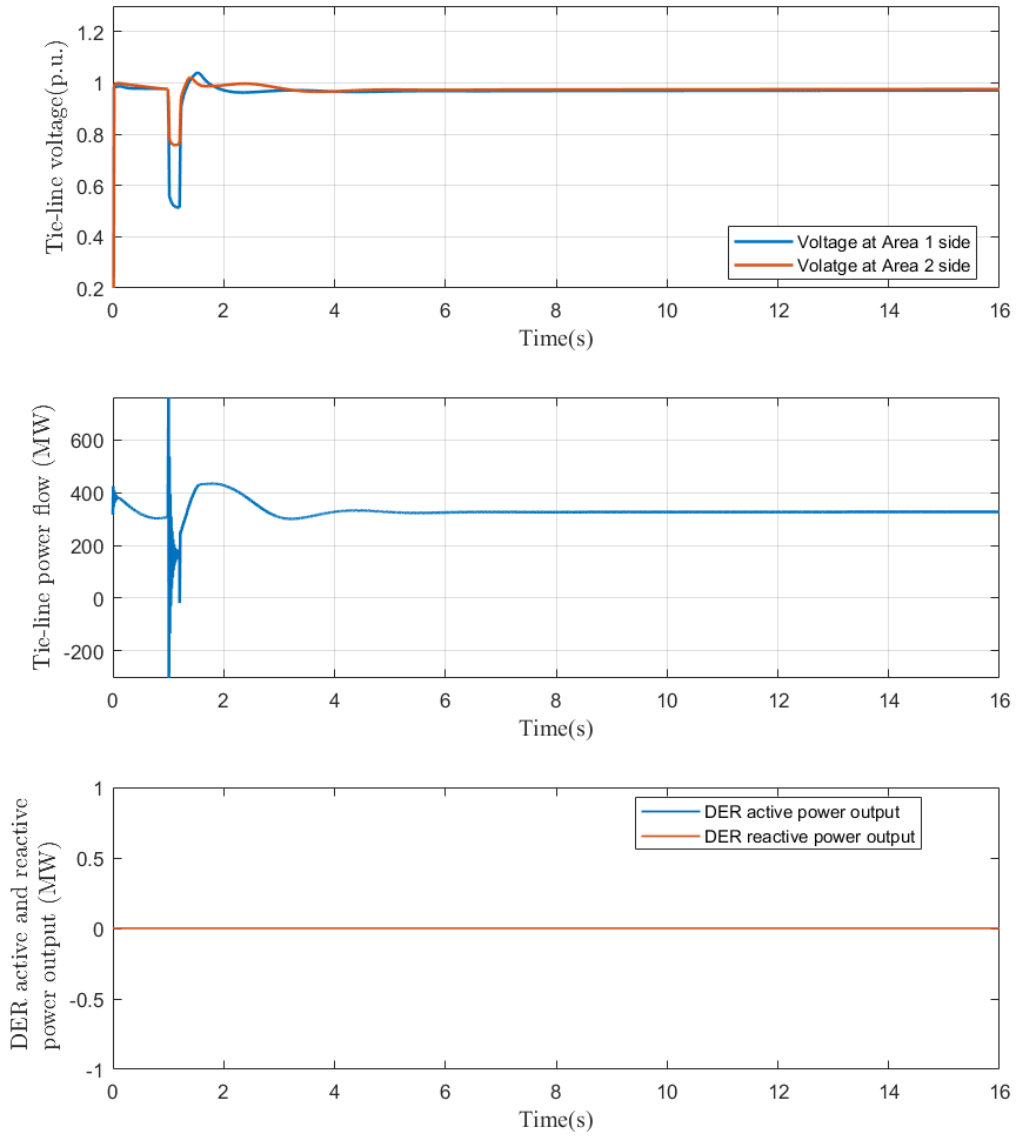

FIGURE 16 System responses following a transmission line fault without DER penetration.

The second scenario is a 16% DER penetration case where DER active power output is at 155 MW. The system responses, including tie-line two-terminal voltages and power flow, DER active and reactive power, DER trigger signal, and frequency and voltage at the DER PCC, were plotted in Figure 17. In this scenario, the transmission-line-fault-induced phenomena include (a) voltage sags both at the two tie-line terminals and the DER PCC; (b) temporary spikes both in the tie-line power flow and DER active and reactive power output; and (c) temporary frequency excursions measured at the DER PCC. The voltage and frequency excursions experienced at the DER PCC were not enough to trigger the DERs offline. As can be seen, after the fault was cleared by the transmission protection devices, all the quantities returned to normal values, and the system maintained stability throughout the entire disturbance.

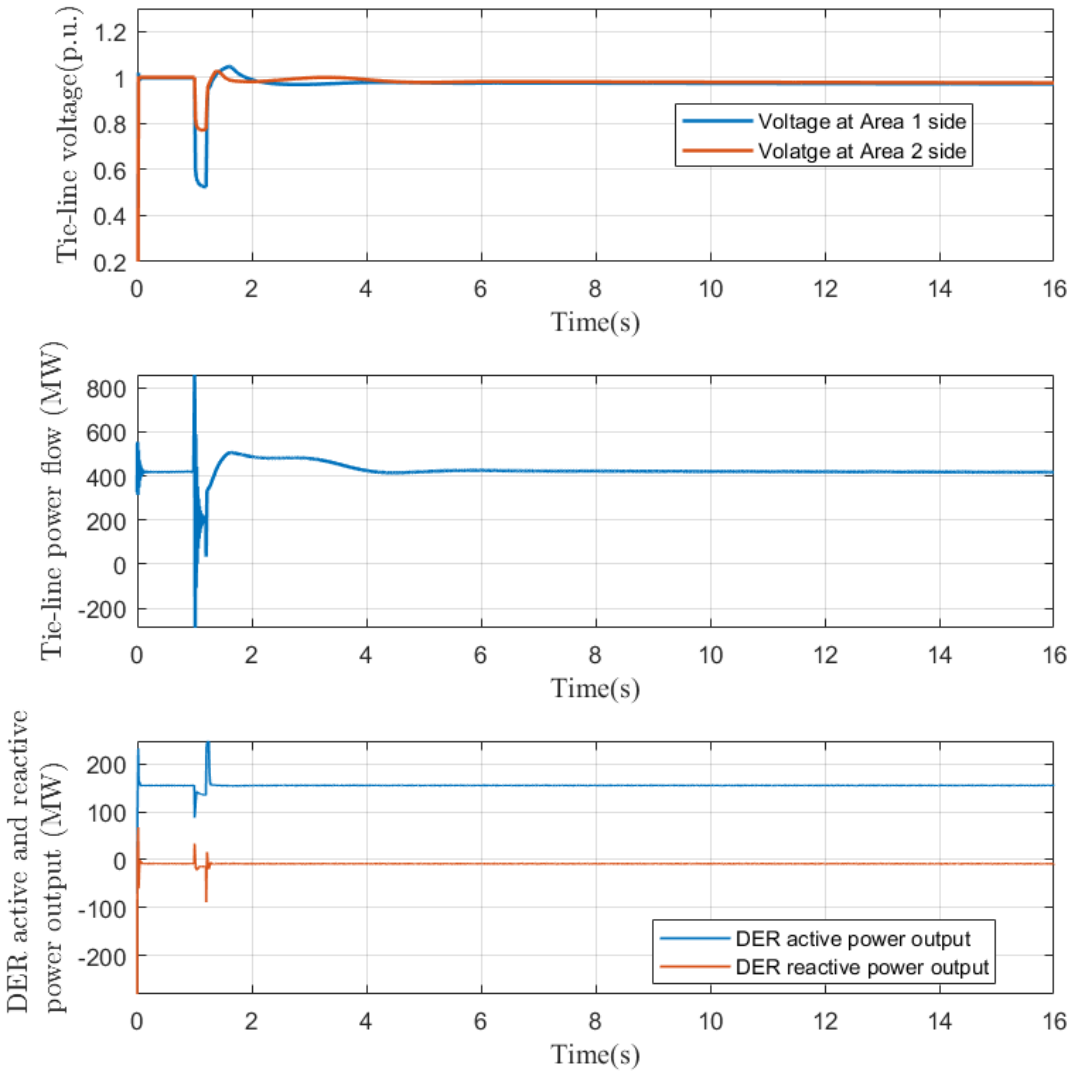

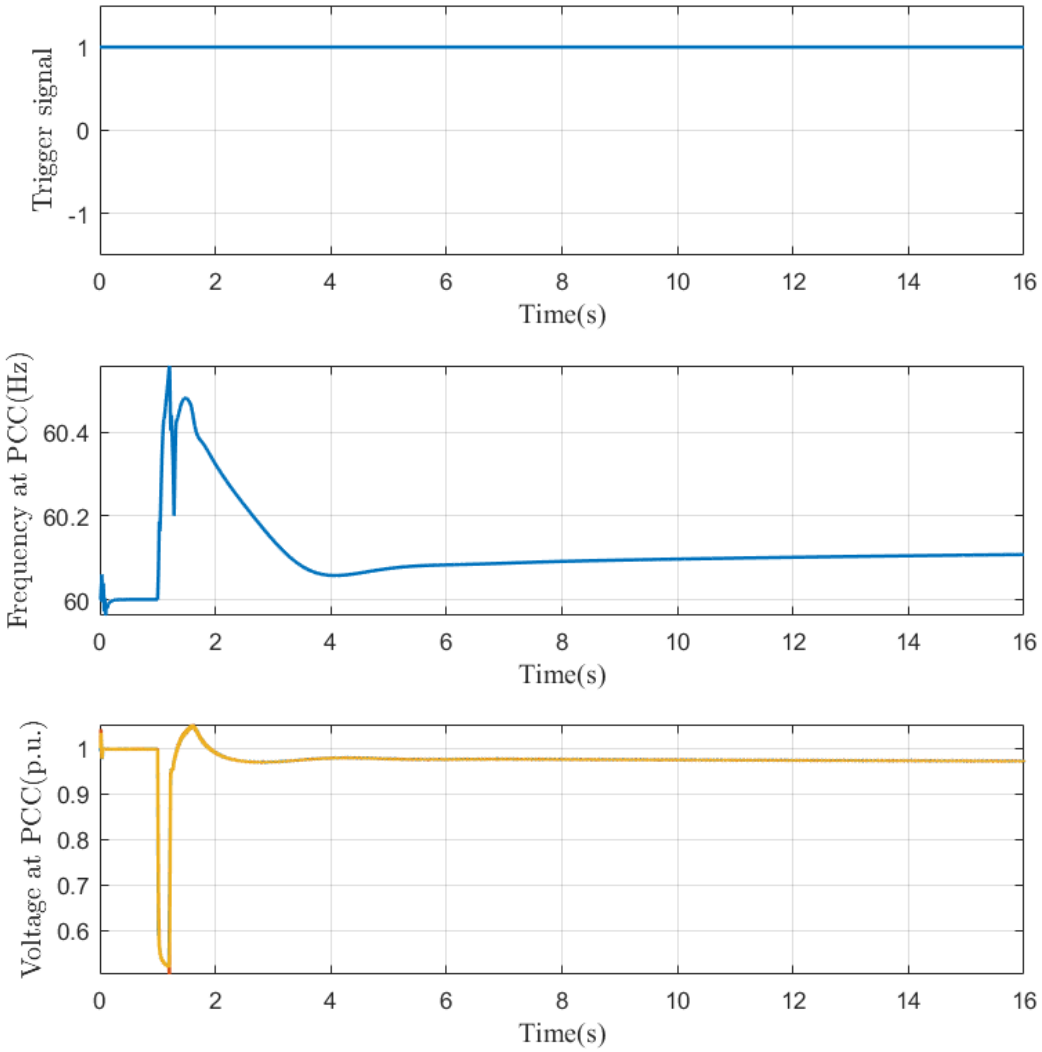

FIGURE 17 System responses following a transmission line fault for 16% DER penetration scenario.

The third scenario is a 33% DER penetration case where the DER active power output is at 315 MW. The system responses are shown in Figure 18. In this scenario, the transmission-line-fault-induced phenomena during the fault exhibited similar characteristics to those in the 16% penetration scenario. After the fault was cleared, continued large frequency and voltage deviations at the DER PCC were observed, and eventually the DERs were tripped offline at 2.35 s as a result of overvoltage protection. Upon the triggering offline of the DERs, the system went through a few cycles of large oscillations, manifested in the tie-line two-terminal voltages and power flow, before eventually returning to normal. During the oscillation period, the system was showing a tendency toward transient instability.

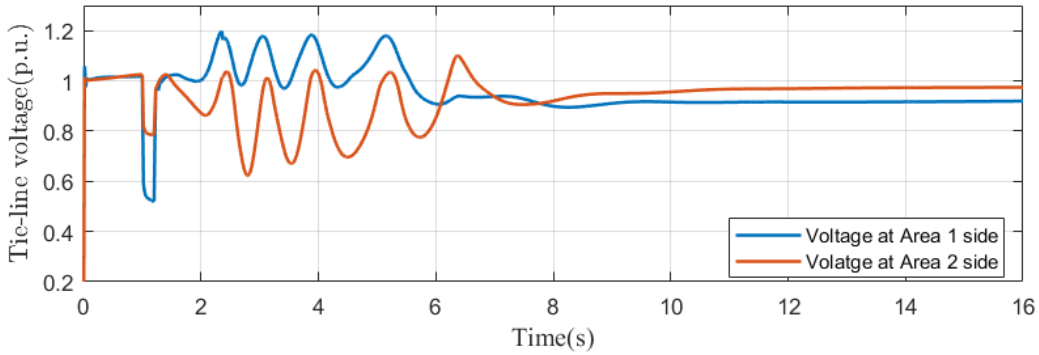
Tie-line voltage(p.u.)
1.2
1
0.8
0.6
0.4
0.2
0
2
4
6
8
10
12
14
16
Time(s)
Voltage at Area 1 side
Volatge at Area 2 side

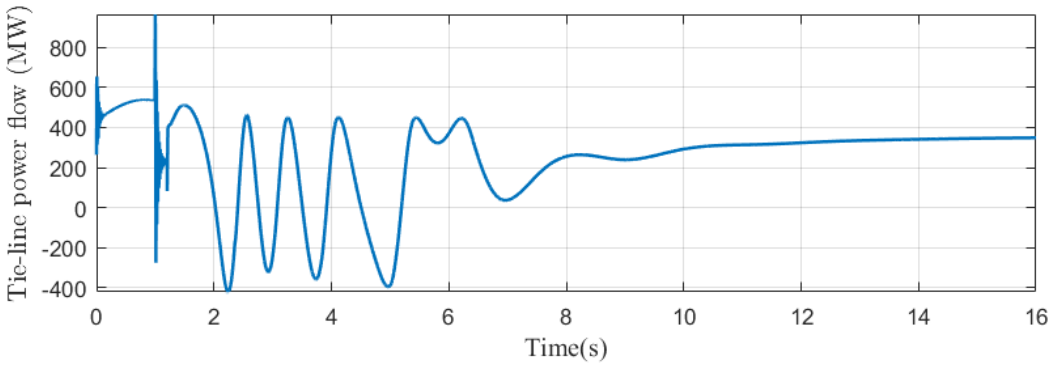
Tie-line power flow (MW)
800
600
400
200
0
-200
-400
0
2
4
6
8
10
12
14
16
Time(s)

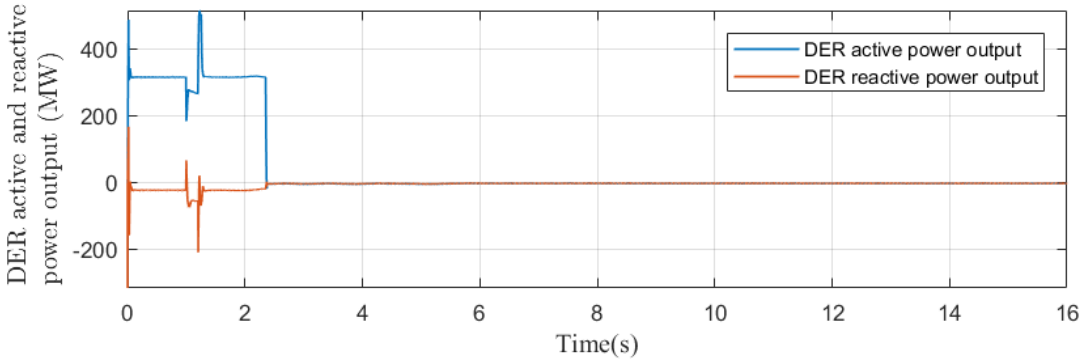
DER active and reactive power output (MW)
400
200
0
-200
0
2
4
6
8
10
12
14
16
Time(s)
DER active power output
DER reactive power output

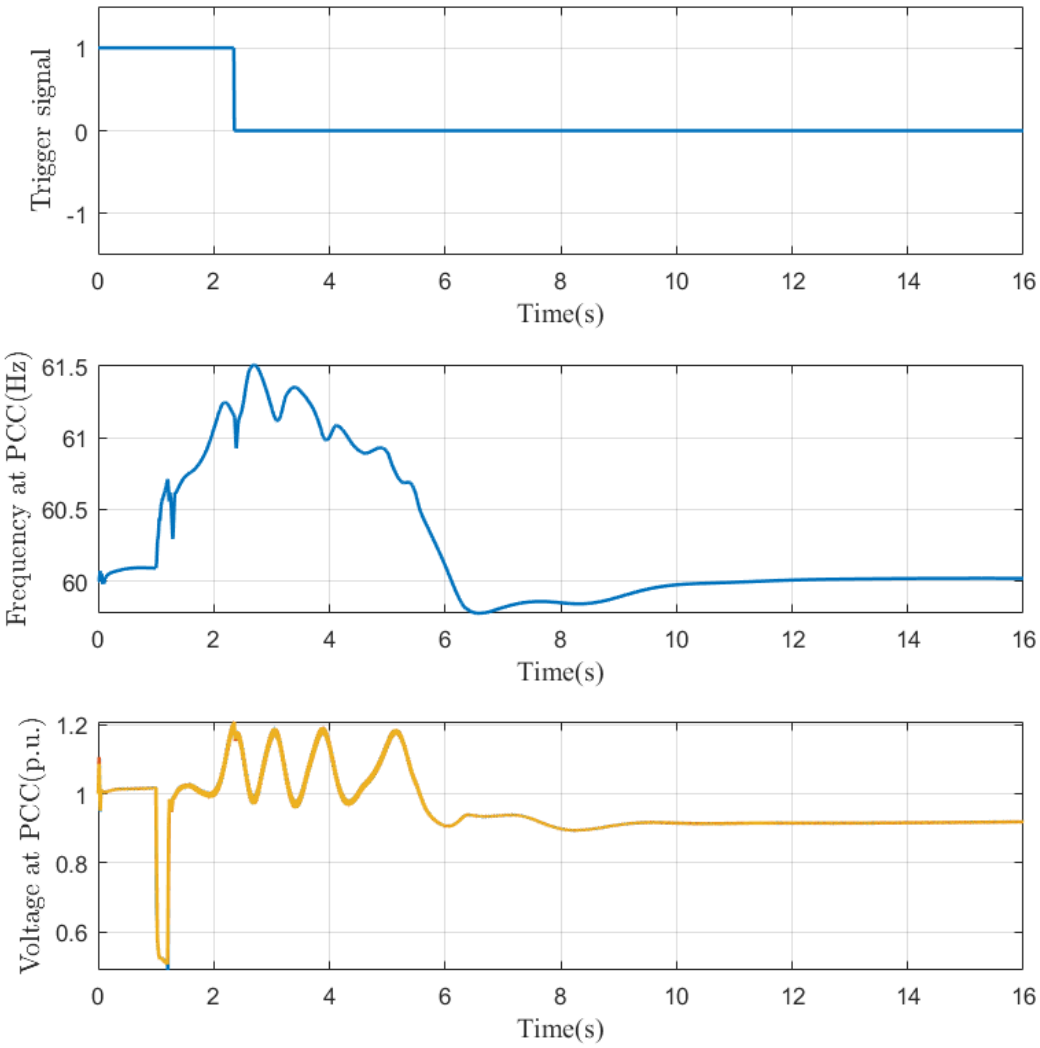

FIGURE 18 System responses following a transmission line fault for 33% DER penetration scenario.

The fourth scenario is a 49% DER penetration case, where the DERs' active power output is at 475 MW. The system responses were plotted in Figure 19. In this scenario, the transmission-line-fault-induced phenomena during the fault exhibited similar characteristics to those observed in the 16% penetration scenario. As in the 33% penetration scenario, after the fault was cleared, continued large frequency and voltage deviations at the DER PCC were observed and eventually the DERs were tripped offline as a result of overvoltage protection. However, in this scenario, the DERs were tripped offline at 2.01 s, 0.34 s earlier than in the previous scenario, because of the larger voltage deviations experienced at the DER PCC. Upon the triggering offline of the DERs, the system went through a few cycles of large oscillations, manifested in the tie-line two-terminal voltages and power flow, before eventually returning to normal. During the oscillation period, similar to the previous scenario, the system was showing a tendency toward transient instability.

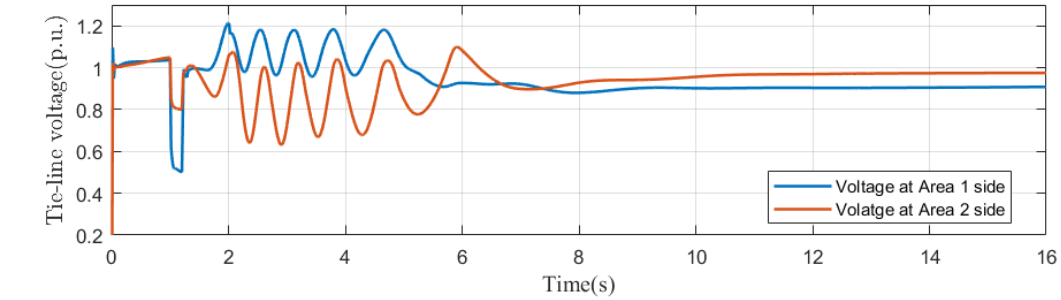
Tie-line voltage(p.u.)
1.2
1
0.8
0.6
0.4
0.2
0
2
4
6
8
10
12
14
16
Time(s)
Voltage at Area 1 side
Volatge at Area 2 side

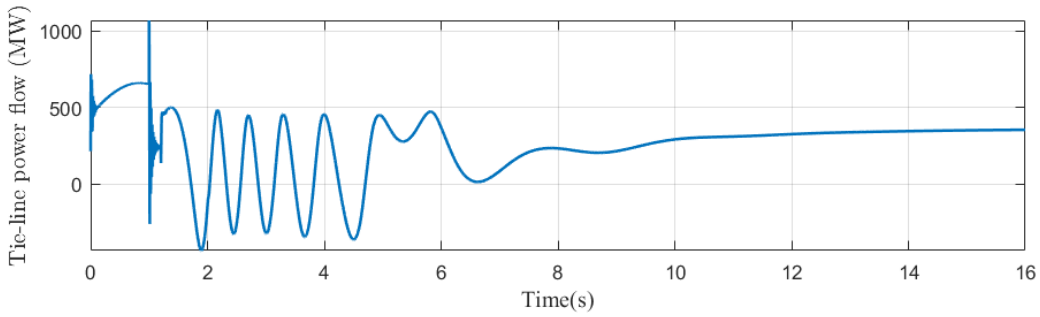
Tie-line power flow (MW)
1000
500
0
0
2
4
6
8
10
12
14
16
Time(s)

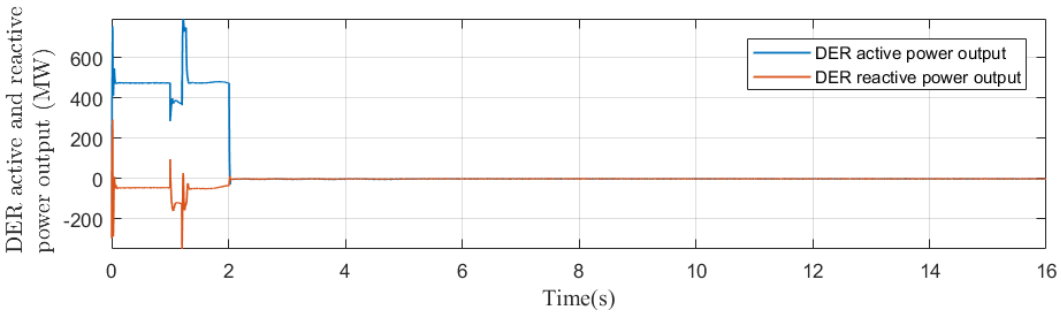
DER active and reactive power output (MW)
600
400
200
0
-200
0
2
4
6
8
10
12
14
16
Time(s)
DER active power output
DER reactive power output

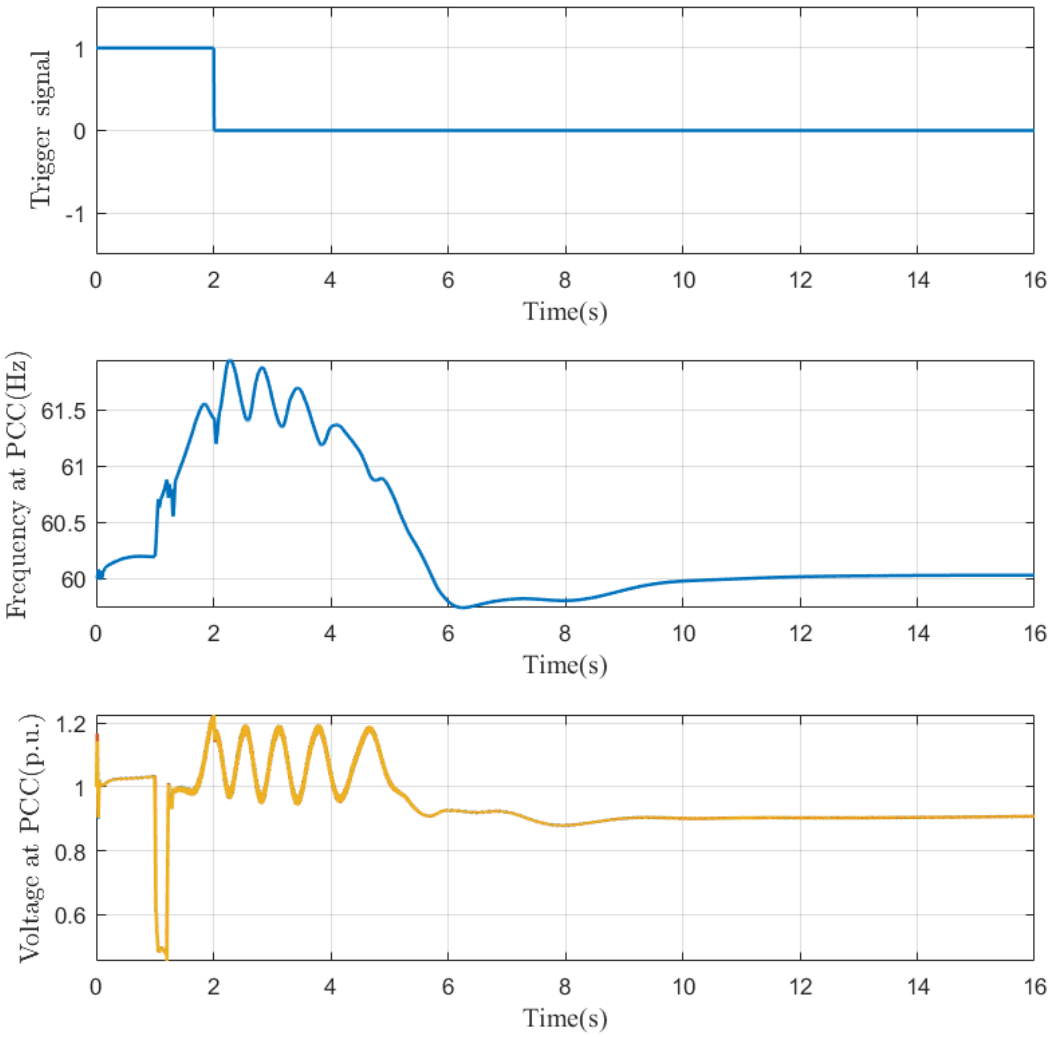

FIGURE 19 System responses following a transmission line fault for 49% DER penetration scenario.

6 SUMMARY AND FUTURE WORK

6.1 ACHIEVEMENTS

The study began with the identification of gaps in DER modeling for BES steady-state studies (power flow analysis and short-circuit analysis) and dynamic studies (disturbance ride-through studies and transient stability studies). Taking into account the caveats identified regarding the state-of-the-art DER modeling techniques, a T&D combined model was developed on the MATLAB/Simulink platform to enable a full investigation of DERs' impact on BES steady-state and dynamic behavior. Kundur Two-Area system was adopted to faithfully represent all the operation modes and dynamics of bulk energy systems. On the distribution side, the IEEE 34-node test feeder was modeled with high penetration of multiple types of DERs, along with interconnection standard implemented in accordance with IEEE Std. 1547a-2014 [13]. This T&D combined model is capable of full-scale static, dynamic and EMT simulations. Three-phase and single-phase DER modeling was developed and integrated into the distribution network. With these features, the T&D combined model can be used by grid planners and operators to evaluate the aggregate effects of unbalanced multi-phase DERs on the T-D interface, understand the level of impact of DERs on the BES reliability, and evaluate advanced control strategies to improve BES reliability.

A key issue hindering large-scale DER deployment has to do with DERs' intermittency and variability, which may result in more frequent and volatile system frequency deviations. If this frequency deviation is more than a certain value, it may have a detrimental impact on system reliability and stability. To overcome this issue and take corrective action, it is essential for the DERs to participate in frequency responses; accomplishing this objective relies on a knowledge of real-time system frequency. Therefore, in this report, a thorough literature survey was conducted on various real-time frequency estimation and prediction techniques for sudden changes in system frequency due to intermittent DERs. On the basis of these estimation and prediction techniques, appropriate actions to provide frequency support were discussed.

Using the MATLAB-based T&D combined model, six benchmark case studies were carried out to investigate DERs' impact on the frequency regulation, voltage stability and dynamic stability of a BES. The results and conclusions from each benchmark case study are summarized as follows:

- Benchmark case 1, "Effect of DERs replacing synchronous machines on inertial and primary frequency response of a BES," found that overall transmission system inertia is reduced as the number of DERs replacing SGs increases. The higher the DER penetration, the higher the initial ROCOF and the lower the frequency nadir upon the disturbance. Higher DER penetration can also result in lower settling frequency in the transmission system, indicating that it is more challenging for the primary frequency control of the responsive SGs to arrest the frequency deviation. Therefore, reduced system inertia may threaten BES stability and mitigation measures to compensate for lost inertia should be considered.

- Benchmark case 2, “Impact of DERs on AGC,” showed that as the level of DER penetration increases, the recovery time for AGC to restore the transmission system frequency becomes longer. It was also observed that larger and longer frequency oscillations occur upon the disturbance for higher DER penetration scenarios. The system’s inability to quickly dampen these big swings could cause more equipment to trip off in order to protect itself, and thus possibly lead to a cascading failure.

- Benchmark case 3, “Impact of DER on load following of a BES,” demonstrated that high DER penetration also creates ramping challenges for the BES, with plots exhibiting similar characteristics to duck curves produced by CAISO.

- Benchmark case 4, “Effect of intermittent DER output on system voltages and frequency,” showed that when the power output of DERs is changing at a certain low frequency, oscillations of the corresponding frequency in system voltage and other measurements can be observed on the power grid. These low-frequency oscillations do not cause the DER protection system to trigger, nor are they damped by PSSs. These low-frequency oscillations may amplify once a contingency event occurs and possibly cause the entire system to collapse.

- Benchmark case 5, “DER impact on the small-signal stability of a BES,” showed that the eigenvalues related to small-signal stability of the BES tend to move to the right half of the s-plane with higher DER penetration, making the system more prone to instability caused by small disturbances.

- Benchmark case 6, “DER impact on the transient stability of a BES,” demonstrated that higher DER penetration conditions may lead to higher peak-to-peak oscillation values, faster DER tripping, and a longer time for the system to return to normal. In other words, more DER penetration may put the power grid at risk of instability after a severe transmission system fault.

These benchmark cases were developed in close collaboration with the NERC’s Essential Reliability Service Working Group and Distributed Energy Resources Task Force. The case studies conducted using the developed T&D combined model will provide guidelines for on-going research in the area of BES impact analysis considering high-penetration DERs.

6.2 FUTURE WORK ON IMPACT ANALYSIS AND RELIABILITY ENHANCEMENT OF BES CONSIDERING HIGH-PENETRATION DERs ON DISTRIBUTION LEVEL

The following next steps are planned in developing the impact analysis and reliability enhancement strategies of BES considering high-penetration DERs on distribution level:

1. Model distribution system protection devices, including circuit breakers, reclosers, fuses, and sectionalizers;

2. Model load tap changers in substation transformers, switched capacitor banks with controls, and voltage regulators in distribution systems;

3. Investigate DERs' impact on and contribution to frequency regulation of BESs. (A detailed work plan can be found in Appendix B.)

4. Investigate DERs' impact on and contribution to voltage stability of BESs. (A detailed work plan can be found in Appendix B.)

5. Monitor DER interconnection standards and understand their implications for the reliability of BESs. (A detailed work plan can be found in Appendix B.)

6.3 FUTURE WORK ON T&D CO-SIMULATION TOOL DEVELOPMENT

It is realized that the T&D combined model developed on the MATLAB platform cannot be scaled to a level of network size that is realistic and meets the computational requirements of the bulk electric system, owing to MATLAB's inherent limitations. To overcome these challenges, one approach is to develop a combined T&D model on another platform that can address the network size and computational complexity issues. However, this approach is highly complex and time-consuming. Another approach is to utilize existing tools for transmission and distribution simulations and integrate them into a full-fledged T&D co-simulation tool.

Given the urgency of the need and available options, a T&D co-simulation tool, potentially coupling PSS®E and EMTP, will be developed in the next phase of this project. PSS®E is adopted on the T side, considering that interconnection, planning coordinator, and balancing authority network models are widely modeled in PSS®E as of today. EMTP is chosen on the D side because of its capabilities to support dynamic and EMT simulations. Once developed, this tool can be adopted by NERC and planning coordinators for day-to-day planning and operations studies for high-DER-penetration scenarios, and can handle real-life scenarios on T&D networks.

Among the many challenges in developing the T&D co-simulation tool, data collection and exchange between T&D and the computational resource requirements stand out. Historically, because of the one-way power flow and passive nature of distribution systems, feeders beyond the distribution substation have been treated as one aggregated load at a node on

the transmission system. There has been no need for transmission simulators to consider detailed distribution systems beyond the transmission node. Distribution utilities have been using dedicated distribution simulators to perform planning and operation studies. Distribution simulators specialize in handling large numbers of nodes existing in the network, especially when the secondary side of service transformers is also modeled, which can amount to the order of 10,000 nodes for a single feeder. For a regular-sized distribution utility, the total number of nodes present in the entire distribution network is easily of the order of magnitude of hundreds of thousands.

Owing to the active nature of modern distribution systems with a high penetration of DERs, transmission system operators and reliability coordinators are seeing the need for more detailed visibility of distribution networks to conduct realistic planning and operational studies that couple the T&D systems. However, T&D utilities are usually separate entities because of the deregulation of electricity markets. In addition, the distribution-side modeling is highly dynamic and voluminous. All of these factors make data collection and exchange between T&D utilities a challenge itself. The explosion in the number of nodes and the exponential increase in the formulation complexities for a T&D co-simulator will certainly necessitate parallel computing algorithms and high-performance computational resources.

The functional requirements for the T&D co-simulation tool, its key attributes for potential applications and analyses, and the technical approach to its development are discussed in Appendix C:

APPENDIX A: SYSTEM DATA DESCRIPTIONS

DISTRIBUTION SYSTEM DATA

For the maximum feeder capacity, the current flowing through the substation is close to 580 A per phase. Keeping a margin for future increments in loads, the transformer and line at the start of the substation is chosen to have an ampacity of 1.25 times the nominal maximum current. Thus, the outgoing line from the substation is chosen to be an aluminum conductor steel-reinforced (ACSR) conductor of size 556.5 kcmil with an ampacity of 726 A. The overhead conductor spacing model and configuration are used, per [49]. The impedance data for different configurations are obtained from [20], [50].

The impedances provided in [20], [50] are in matrix form in terms of self-impedance and mutual impedance. In this work, the equivalent positive- and zero-sequence impedances are computed for each of the line configurations using the equations provided in [51]. For example, the resistance matrix for configuration 601 in [50] is given as

$$R = \begin{bmatrix} R_{s11} & R_{m12} & R_{m13} \\ R_{m12} & R_{s22} & R_{m23} \\ R_{m13} & R_{m23} & R_{s33} \end{bmatrix}$$

Assuming the lines are transposed at even distances, the positive- and zero-sequence resistances are computed as

$$R_1 = \bar{R}_s - \bar{R}_m$$
$$R_0 = \bar{R}_S + 2\bar{R}_m$$
$$\bar{R}_s = (R_{s11} + R_{s22} + R_{s33})/3$$
$$\bar{R}_m = (R_{m12} + R_{m13} + R_{m23})/3$$

where R_1 is the positive-sequence resistance, R_0 is the zero-sequence resistance, $\bar{R}_s$ is the average self-resistance, and $\bar{R}_m$ is the average mutual resistance.

A. Overhead Line Configuration Data

Overhead line configuration data are given in Table 13. More details about the overhead spacing models and conductors can be obtained from [49].

TABLE 13 Overhead Line Configuration Data

Config.	Phasing	Phase	Neutral	Spacing	Ampacity
		ACSR	ACSR	ID	amps
601	BACN	556.50 26/7	4/0 6/1	500	726
602	CABN	4/0 6/1	4/0 6/1	500	357
603	CBN	1/0	1/0	505	242
604	ACN	1/0	1/0	505	242
605	CN	1/0	1/0	510	242
300	BACN	1/0	1/0	500	242
301	BACN	#2 6/1	#2 6/1	500	184
302	AN	#4 6/1	#4 6/1	510	140
303	BN	#4 6/1	#4 6/1	510	140
304	BN	#2 6/1	#2 6/1	510	184

B. Underground Cable Configuration Data

Underground cable configuration data are given in Table 14. More details about the underground cable spacing models and cables can be obtained from [49].

TABLE 14 Underground Cable Configuration Data

Config.	Phasing	Phase	Neutral	Spacing	Ampacity
		ACSR	ACSR	ID	amps
606	ABCN	250.0 AA, CN	None	515	260
607	AN	1/0 AA, TS	1/0 Cu	520	165

C. Line Segment Data

Details about the distribution line and cable connectivity, length, and configuration are provided in Table 15. The node diagram of the test system is given in Figure 20.

TABLE 15 Line Segment Data

Node A	Node B	Length (miles)	Config.
1	2	0.5	601
2	3	0.5	601
3	4	0.5	301
3	5	0.4	601
5	6	0.4	602
5	7	0.35	602
6	61	0.5	602
61	62	0.25	602
62	63	0.35	602
62	621	0.4	606
621	622	0.3	606
622	623	0.3	606
63	64	0.5	602
64	65	0.25	300
64	641	0.3	300
641	642	0.5	300
642	643	0.5	300
643	644	0.3	300
644	645	0.5	300
645	646	0.35	300
646	647	0.35	606
647	648	0.25	606
65	66	0.4	301
66	67	0.25	606
7	71	0.3	602
71	72	0.35	602
72	73	0.3	300
72	721	0.5	301
721	722	0.3	301
722	723	0.4	301
73	74	0.4	300
74	75	0.35	300
75	76	0.4	300
76	761	0.4	301
761	762	0.5	301
76	77	0.4	301
77	78	0.6	301
78	79	0.25	301
78	781	0.25	606
781	782	0.3	606

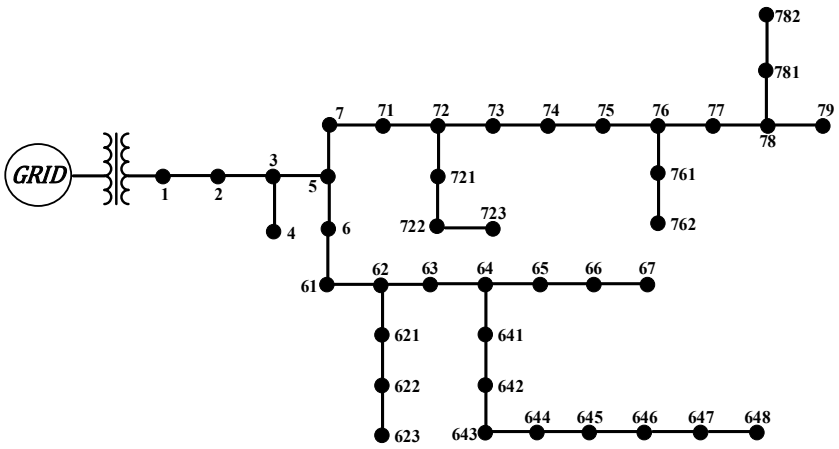

FIGURE 20 Node diagram of the IEEE 34-node test feeder.

D. Spot Load Data

Spot load data are given in Table 16.

TABLE 16 Spot Load Data

Node	Load Type	MW	MVAR
2	Y-PQ	0.563	0.434
4	Y-Z	0.1957	0.1206
5	Y-Z	0.1505	0.117
6	D-PQ	0.2423	0.1883
7	Y-Z	0.2496	0.1940
61	Y-I	0.1034	0.0804
62	D-Z	0.1157	0.0899
63	Y-Z	0.1157	0.0899
64	Y-Z	0.3683	0.1661
65	D-I	0.125	0.067
67	Y-PQ	0.0393	0.0305
72	Y-Z	0.636	0.49
73	Y-PQ	0.0572	0.044
74	D-Z	0.2737	0.1913
75	Y-PQ	0.3891	0.299
79	D-Z	0.3286	0.1920
642	D-PQ	0.144	0.112
623	Y-Z	0.3195	0.2015
641	D-PQ	0.0144	0.0112
643	Y-I	0.0901	0.0702
646	Y-PQ	0.1597	0.1241
648	Y-Z	0.0123	0.0081
66	Y-PQ	0.103	0.055

TABLE 16 (Cont.)

Node	Load Type	MW	MVAR
761	Y-I	0.1701	0.0967
762	Y-PQ	0.1279	0.0994
721	D-PQ	0.0636	0.049

E. Distributed Load Data

Distributed load data are given in Table 17.

TABLE 17 Distributed Load Data

Node A	Node B	Load Type	MW	MVAR
2	3	Y-Z	0.2199	0.1513
71	72	D-Z	0.1936	0.1055
76	761	D-Z	0.2207	0.1055
78	781	Y-I	0.1687	0.1311
621	622	Y-Z	0.1615	0.1255
644	645	D-PQ	0.3082	0.2395
647	648	Y-Z	0.2321	0.1804
722	723	Y-PQ	0.1707	0.1327
781	782	Y-Z	0.6047	0.4197

F. Capacitor Data

Capacitor data are provided in Table 18.

TABLE 18
Capacitor Data

Node	MVAR
645	0.9
63	0.3
71	0.6
77	1.8

THREE-PHASE DER SYSTEM DATA

In the following subsections, the details of each of the three-phase DERs are discussed.

Diesel Generator

Diesel generator units are one of the most highly used backup power sources in industrial and commercial buildings. These units can be generally controlled in speed control mode to maintain the frequency close to the nominal rated frequency based on power grid standards. These units are also equipped with their own governor and excitation system. Owing to their large capacity, they can be used as a grid-forming generator in a microgrid setup. The specifications of a diesel generator unit are provided in Table 19.

TABLE 19 Parameters for 3.125-MVA Diesel Generator

Parameter	Value
Diesel Generator Parameters	
Nominal Power	$3.125 \times 10^6\ VA$
Nominal Line-to-Line Voltage	2400 V
Nominal Frequency	60 Hz
Reactances $[X_d, X'_d, X''_d, X_q, X''_q, X_l]$	[1.56, 0296, 0.177, 1.06, 0.177, 0.052]
Time Constants $[T'_d\ T''_d\ T''_q]$	[0.024, 0.006, 0.006] s
Stator Resistance (R_s)	0.0036 p.u.
Inertia Coefficient (H)	1.07 s
Pole Pairs (p)	2
Friction Factor (F)	0 p.u.
Excitation System Parameters	
Excitation System Type	IEEE AC1A
Low-Pass Filter Time Constant (T_r)	$20\ e^{-3}$ s
Voltage Regulator Gain and Time Constant $[K_a\ T_a]$	[400, 0.2 s]
Damping Filter Gain and Time Constant $[K_f\ T_f]$	[0.03, 1.0 s]
Transient Gain Reduction Lead and Lag Time Constants $[T_b\ T_c]$	[0, 0] s
Diesel Engine Governor	
Regulator Gain (K)	40
Regulator Time Constants $[T_1\ T_2\ T_3]$	[0.01, 0.02, 0.2] s
Actuator Time Constants $[T_4\ T_5\ T_6]$	[0.25, 0.009, 0.0384] s
Engine Delay (T_d)	0.024 s

The diesel engine governor system is modeled using a series combination of controller, actuator and engine transfer functions. The controller, actuator and engine transfer functions are as follows:

$$H_{controller} = \frac{K(1 + T_3 s)}{1 + T_1 s + T_1 T_2 s^2}$$

$$H_{actuator} = \frac{1 + T_4 s}{s(1 + T_5 s)(1 + T_6 s)}$$

$$Engine = Time\ Delay\ of\ 0.024\ seconds$$

When the diesel generator is operated in the grid-connected mode, the reference speed is maintained at the nominal system speed and the reference voltage is maintained at the nominal system voltage of 1 p.u.. However, when the diesel generator is operating in the droop control mode, the reference speed provided to the diesel engine governor and the reference voltage provided to the excitation system are updated using the droop control as follows:

$$\omega = \omega^* - K_p(P - P_{nom})$$

$$V = V^* - K_q(Q - Q_{nom})$$

Finally, the diesel generator is connected to the distribution system using a 2.4-kV D/12.47-kV Yg, 3.5 MVA, R = 0.03%, X = 6% transformer.

Wind Turbine Generator

The WTG is modeled using a single Doubly Fed Induction Generator (DFIG) of 1.5 MVA capacity. In order to model the wind farm with a larger capacity, the same model can be used, but with parameters scaled proportionally to represent the aggregated model of the farm. A typical variable-speed wind energy conversion system (WECS) based on the DFIG is shown in Figure 21. A DFIG-based WECS has a rotor-side converter (RSC) and a grid-side converter (GSC) separated by a DC link capacitor. The GSC maintains the DC link voltage at a steady value, and the RSC is used to control the active and reactive power generation from the DFIG. The mechanical torque input to the DFIG is obtained from the wind turbine coupled to the DFIG through a gearbox.

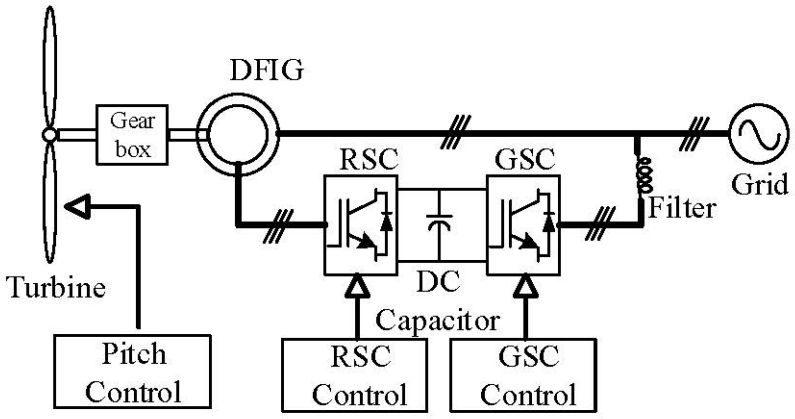

FIGURE 21 Typical configuration of DFIG-based WECS.

The mechanical power and torque that a wind turbine extracts from the wind is calculated by means of the following equations [52]–[53]:

$$P_m = \frac{1}{2}\rho A v_\omega^3 C_p(\lambda, \beta) = f(v_\omega, \omega_t)$$

$$T_m = \frac{P_m}{\omega_t}$$

$$\lambda_r = \frac{1}{\lambda + 0.08\beta} - \frac{0.035}{\beta^3 + 1}$$

$$C_p = c_1(c_2\lambda_r - c_3\beta - c_4)e^{-c_5\lambda_r} + c_6\lambda$$

$$\lambda = \frac{\omega_t \times R}{v_\omega}$$

where $c_1 = 0.52$, $c_2 = 116$, $c_3 = 0.4$, $c_4 = 5$, $c_5 = 21$, and $c_6 = 0.0068$. The details about modeling a wind turbine can be obtained from [52]–[53].

In the above equations, P_m is the mechanical power (watts), ρ is the air density (taken as 1.215 kg/m^3), A is the swept area of the turbine blades (m^2), v_ω is the wind speed (m/s), C_p is the wind turbine power coefficient, β is the pitch angle (degree), ω_t is the angular velocity of the turbine (rad/s), R is the rotor radius (m), and λ is the tip speed ratio (TSR).

Figure 22 shows the typical mechanical power output vs rotor speed profile for various wind speeds. It can be observed that for a fixed wind speed, there is a particular rotor speed from which maximum power extraction can be ensured—if the DFIG is operated. The trajectory of

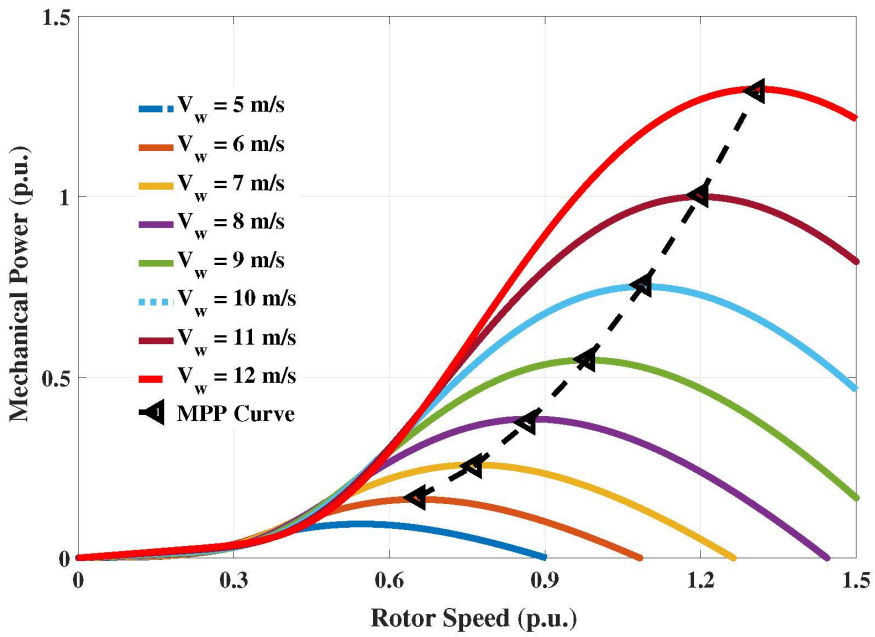

FIGURE 22 Mechanical power output of a wind turbine as a function of rotor speed and wind velocity.

such rotor speed in the power vs rotor speed profile curve is shown in Figure 22. The value of TSR, λ, is constant for all maximum power points. The optimum TSR and the maximum value for power coefficient C_p for a particular wind turbine can be obtained from the family of power coefficient vs TSR curves plotted for different values of pitch angle β (not shown here). For the wind turbine model selected in this work, the optimum TSR and maximum value of power coefficient are 8.1 and 0.482, respectively.

The wind farm model designed for this study includes all the major components of the WTG system, such as the GSC, RSC, pitch controller, and a two-mass model of turbines. The DFIG is controlled using a conventional vector control technique in a stator-flux-oriented reference frame, and it is assumed that the grid-side voltage is available for synchronizing the wind turbine system with the grid as shown in Figure 23. The vector control employs current control on the inner loop, and on the outer loop, active and reactive power (can also be voltage, power factor) are controlled. The goal of the GSC is to control the DC link voltage between the RSC and GSC and to control the reactive power exchange between the GSC and the grid. The goal of the pitch controller is to pitch the rotor blades in such a way that the mechanical stress in the turbine can be reduced during periods of high winds and to maintain the nominal pitch over the allowed wind-speed range so that the maximum power can be extracted. At higher wind speeds, the pitch controller limits the rotor speed to 1.2 p.u. and the maximum power extracted to 1 p.u.. However, the pitch controller can also be used to limit the power extracted from wind energy at normal wind speeds in order to reserve an energy buffer which can be utilized for grid frequency support.

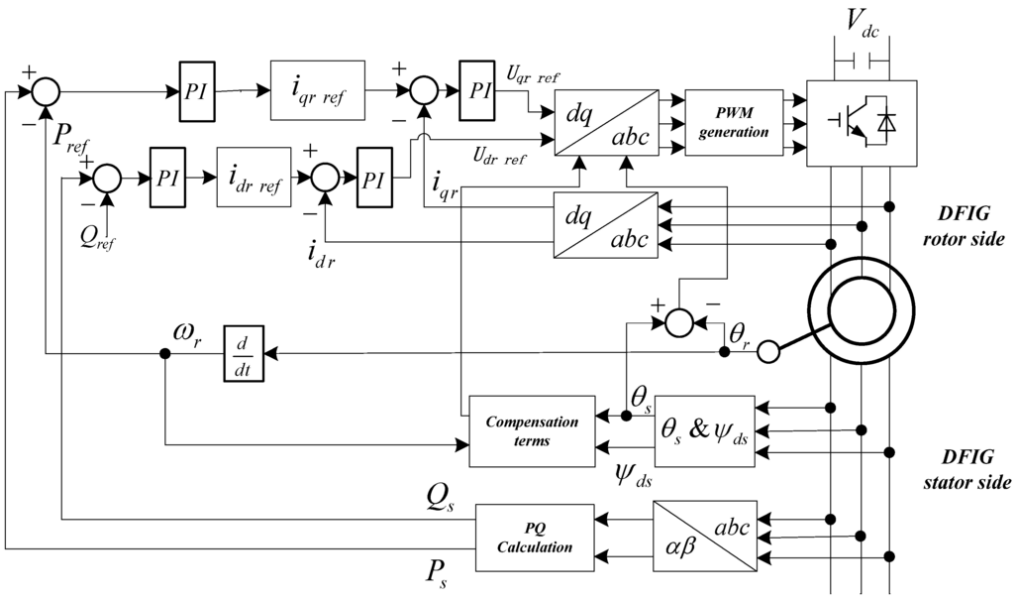

FIGURE 23 Vector control for DFIGs.

The wind farm operates at the maximum power point tracking mode, which means that the active power output of the wind farm is dependent on the available wind velocity. For reactive power output, it can be in either voltage control mode, reactive power control mode, or constant power factor control mode.

The parameters of the DFIG-based WTG system are given in Table 20. The wind farm is connected to the distribution system using a 575-V Yg/12.47-kV Yg, (N_t×2.25) MVA, R = 1%, X = 7% transformer.

TABLE 20 Parameters for 1.5-MVA DFIG-based Wind Turbine System

Parameter	Value
Diesel Generator Parameters	
Number of Turbines (N_t)	1
Nominal Power	$1.5 \times 10^6 \times N_t\ VA$
Nominal Line-to-Line Voltage	2400 V
Nominal Frequency	60 Hz
Stator Resistance and Inductance [R_s, L_{ls}]	[0.0071 0.1714] p.u.
Rotor Resistance and Inductance (ref. to Stator) [R'_r, L'_{lr}]	[0.005 0.1563] p.u.
Mutual Inductance (L_m)	2.9 p.u.
Generator Inertia (H)	0.5 s
Pole Pairs (p)	3
DC Link Capacitor (C_{dc})	$5600 \times N_t\ \mu F$
Coupling Inductor for GSC (L_{GSC})	$1.2/N_t\ mH$

TABLE 20 (Cont.)

Parameter	Value
Turbine Drive Train Parameters	
Wind Turbine Inertia Constant (H)	3.5 s
Shaft Spring Constant (K_s)	2.32 p.u.
Shaft Mutual Damping (K_d)	2 p.u.
Shaft Base Speed	$2\pi \times 60/p$
Turbine Gear Ratio	59.235
Rotor Blade Diameter	70 m

Battery Energy Storage System

The BESS consists of a battery bank rated at 360 kW, 828 kWh, and 720 V DC terminal voltage. The inverter is rated at 540 kVA to provide the required reactive power support to the distribution feeder. The BESS can be given power commands, based on which the battery can be charged or discharged. The battery is connected to the DC link of the inverter through a bi-directional DC/DC converter that maintains the DC link voltage of the inverter. The inverter then sends/absorbs the active/reactive power to/from the grid based on the power references provided to it.

The discharge characteristics of the battery are shown in Figure 24, and the parameters used for BESS modeling are given in Table 21.

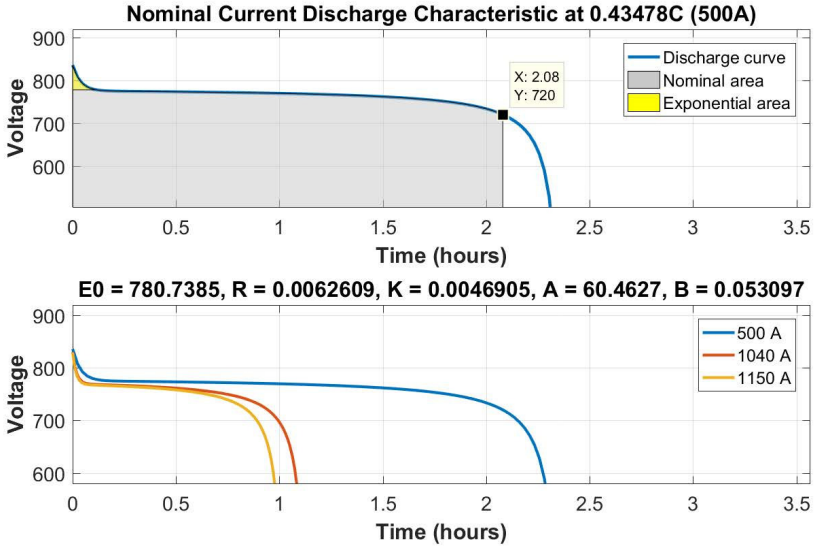

FIGURE 24 Nominal current discharge characteristics of the battery bank used.

TABLE 21 Parameters for 5.4-kVA Battery Energy Storage System

Parameter	Value
Battery Bank Parameters	
Type	Lithium
Nominal Voltage	720 V
Rated Capacity	1.15 kAh
DC/DC and DC/AC Converter Parameters	
Rated Power Capacity	5.4 kW
Inductor	0.1 mH
DC Link Capacitor	0.47 F
Coupling Inductor for Inverter	0.34 mH

The DC/AC converter is controlled using the conventional vector control technique. In the case of islanded operation, when diesel generators are the primary source of energy in the microgrid, BESSs can provide droop-based active and reactive power to support the microgrid frequency and voltage. The droop control implemented in this case is of the following form:

$$P = P_{nom} + K_p \times (\omega - \omega^*)$$

$$Q = Q_{nom} + K_Q \times (V - V^*)$$

The BESS is connected to the distribution system using a 575-V Yg/12.47-kV Yg, (N_t×2.25) MVA, R = 1%, X = 7% transformer.

Photovoltaic System

The PV system consists of PV modules modeled using an aggregated module of 1 MW, a DC/DC converter to extract the maximum power from the PV array, and a three-phase DC/AC inverter to transfer the extracted DC power to the AC grid. The Power-Voltage (P-V) and Current-Voltage (I-V) characteristics of the aggregated 1 MW PV module used are shown in Figure 25. The DC/AC inverter is rated at 1.5 MVA and is controlled in vector control mode.

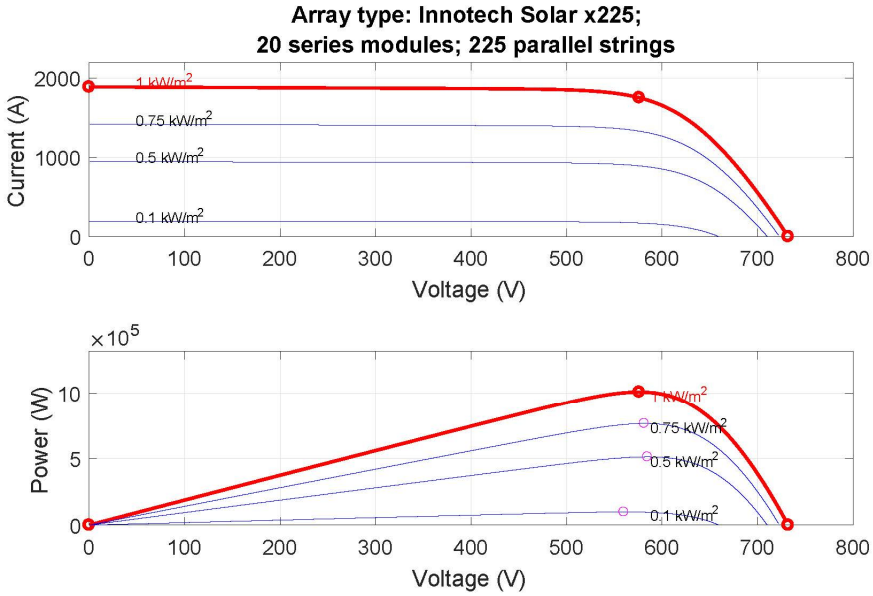

FIGURE 25 P-V and I-V characteristics of the 1-MW-equivalent PV system used.

The parameters for the PV array are given in Table 22. The PV farm is connected to the distribution system using a 575-V Yg/12.47-kV Yg, (N_t×2.25) MVA, R = 1%, X = 7% transformer.

TABLE 22 Parameters for 1-MW PV Array

Parameter	Value
Parallel Strings	225
Series-connected Modules per String	20
Module Used	Innotech Solar x225
PV Terminal Capacitor	0.1 F
DC/DC Converter's Inductor	0.4 mH
DC Link Capacitor	0.1 F
Inverter Coupling Inductor	0.18 mH

SINGLE-PHASE DER SYSTEM DATA

Hysteresis Control-based Single-Phase Inverter

The control scheme for the hysteresis control-based single-phase inverter is shown in Figure 26. The single-phase PV system and BESS are designed for 1.42-kVA and 230-V levels.

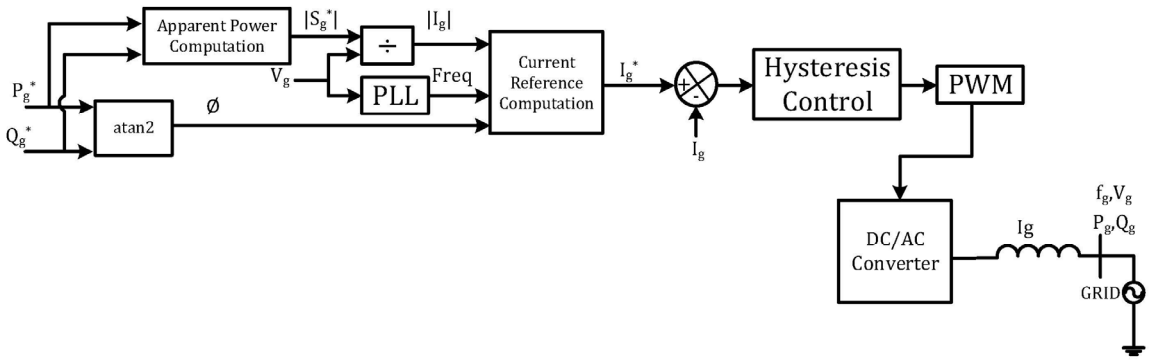

FIGURE 26 Control technique implemented for single-phase inverter system.

DQ Reference-Frame-Control-based Single-Phase Inverter

The control scheme for the DQ reference-frame-control-based single-phase inverter is shown in Figure 27. The parameters for the single-phase DER system are listed in Table 23.

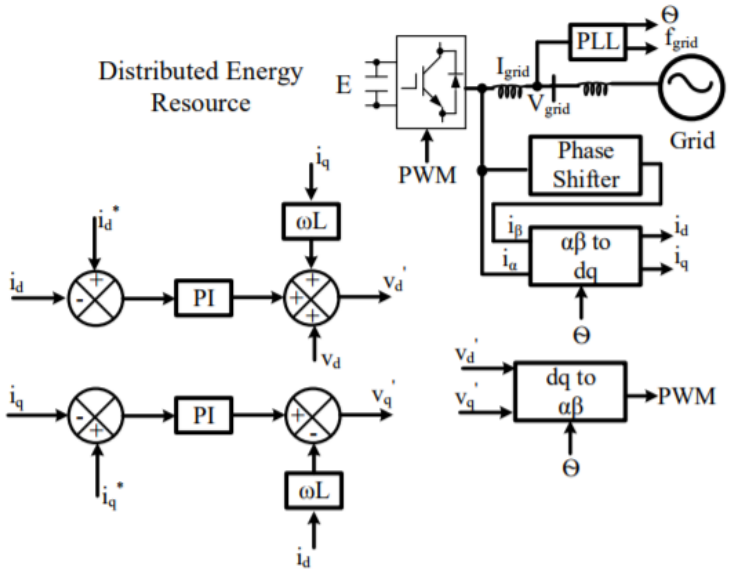

FIGURE 27 DQ reference-frame-based control technique implemented for single-phase inverter system.

TABLE 23 Parameters for 1.5-kW Single-Phase DER

Parameter	Value
Nominal Voltage	230 V
Nominal Current	6.5 A
DC Link Voltage	400 V
Output Filter Inductance	3 mH
Output Filter Capacitance	2.2 μF
PI controller	$K_p = 0{,}1, K_i = 10$

APPENDIX B: WORK PLAN FOR IMPACT ANALYSIS AND RELIABILITY ENHANCEMENT OF BES CONSIDERING HIGH-PENETRATION DERs ON DISTRIBUTION LEVEL

The detailed work plan to investigate the DERs' impact on and contribution to the frequency regulation and voltage stability of a BES, and to monitor DER interconnection standards and understand their implications for the reliability of a BES, is presented here. It comprises three main tasks, as follows:

(a) Investigation of DERs' impact on and contribution to frequency regulation of a BES, with the following subtasks:

1. Comparison of the impact on BES frequency regulation from aggregated unbalanced multi-phase DERs with those from WECC's PVD1 and Composite Load Model with Distributed PV (CMPLDWG), considering DER ride-through capabilities.

2. Study of the impact of coordination between DER and conventional generators on BES frequency regulation.

3. Analysis of the optimal aggregation of different types of DERs and storage to mitigate the influence of DER intermittency on frequency deviation by controlling DER inverters.

4. Investigation of the characteristics of conventional synchronous machines that can be emulated using a DER inverter.

5. At the primary frequency control level, analysis of role of the virtual-synchronous-machine-based control algorithms for the DER inverter in enhancing its frequency regulation capability.

6. At the secondary frequency control level, defining the control strategy for AGC so as to keep the area control error within acceptable limits following random variations in DER output.

7. Study of the potential contribution of DERs on load following.

(b) Study of DERs' impact on and contribution to voltage stability of a BES, with the following subtasks:

1. Identification of the possible normal-operation scenarios in which the interactions between DER inverters' Q-V controllers and conventional voltage-regulating devices, such as substation load tap changers (LTCs), switched capacitor banks, and voltage regulators, may lead to voltage

oscillation in distribution systems and potential impact on BES voltage stability.

2. Analysis of the DERs' impact on the voltage stability of a BES following transmission disturbance. Development of strategies using DER reactive power to reduce load to stabilize BES voltage following transmission disturbances. Comparison of the effectiveness of classical voltage regulation schemes using LTCs and the new scheme using regulation of DER reactive power in stabilizing the system voltage. Comparison of the impact on BES voltage stability from aggregated unbalanced multi-phase DERs with those from WECC's PVD1 and CMPLDWG.

3. Evaluation of the contribution of DERs' reactive power to the BES voltage control, considering DER ride-through capabilities.

(c) Monitoring DER interconnection standards and understanding their implications for the reliability of a BES, using the following steps:

1. Modification of the implemented DER interconnection model in accordance with the ongoing revision of IEEE Std. 1547 governing DER interconnection requirements, especially the frequency and voltage ride-through requirements.

2. Determination of the appropriate DER fault ride-through settings that ensure bulk system reliability and satisfy distribution-system safety requirements (i.e., prevention of unintentional utility islanding) simultaneously.

3. Investigation of the impact of high DER penetration on coordination among distribution-system protection devices.

4. Investigation of the impact on protection coordination between distribution-system protection devices and DER protection relays with various fault ride-through capabilities.

APPENDIX C: FUNCTIONAL REQUIREMENTS, APPLICATIONS, AND DEVELOPMENT PLAN FOR T&D CO-SIMULATION TOOL

The functional requirements for the T&D co-simulation tool, its key attributes for potential applications and analyses, and the technical approach to its development are discussed in detailed here.

The functional requirements of the T&D co-simulation tool are as follows:

1. Capability to
   - Model multi-phase DERs in a distribution system; and
   - Carry out steady-state and dynamic simulations.

2. Capability to model the interface between the transmission and distribution systems up to a 115-kV transmission system (to study effects of the DERs on the BES at multiple voltage levels).

3. Scalability and capability to model realistic single or multiple interconnections such as WECC and East Interconnection and to conduct inter-area studies. Capability to model zoomed-in portions of an interconnection serving a well-defined distribution utility within those boundaries.

4. Flexibility to implement DER interconnection standards such as IEEE Std. 1547 on DER interconnection models. This flexibility can facilitate BES disturbance ride-through studies with expanded frequency and voltage ride-through ranges.

5. Flexibility to implement advanced DER control functions such as Q-V and P-F control to help assess the potential for improving BES reliability.

The efficacy of the tool will be substantiated by its use for multiple applications and analyses. Specifically, the steady-state simulations will enable the following analyses:

1. Short-term and long-term BES planning studies including power flow analysis, short-circuit analysis, and contingency analysis.

2. BES voltage stability studies following small disturbances.

The dynamic simulations will reinforce the following analyses:

1. BES voltage stability studies following large disturbances such as faults or loss of load or generator.

2. Dynamic stability analysis, including small-signal stability and transient stability.

3. Frequency stability analysis, including inertial frequency response, primary frequency response, and spinning reserve.

4. BES protection studies.

5. BES disturbance ride-through studies.

In conjunction with other operational software or applications, the tool should be able to carry out operational studies for BESs, including the following:

1. Impact on the system's secondary frequency response, typically controlled through the system operator's AGC.

2. Impact on the load following or ramping requirements throughout the day and over the course of seasons, through economic dispatch.

The T&D co-simulation tool will comprise a transmission simulator, a distribution simulator, an interface module linking T&D simulators with sockets and interaction protocols, and a synchronization module.

1. PSS®E, which is an off-the-shelf positive-sequence dynamic simulator, is a potential option for the transmission simulator.

2. EMTP, which is a three-phase unbalanced distribution system dynamic simulator, is a potential option for the distribution simulator.

3. The interface that links T&D simulators is based on Argonne's existing platform is adopted. It has the following features:

    - This platform contains sockets that enable simulators running on different operating systems (e.g., Linux and Windows) to communicate and exchange data.

    - This interface passes along and iterates information (voltages, currents, and powers) between T&D simulators through loosely coupled or tightly coupled protocols. In loosely coupled methods, there is a one-step lag in information exchange between transmission and distribution, but less computation is required. Tightly coupled methods maintain consistency of the boundary conditions at the T&D interface at each time step, but require more computational effort. Different choices of methods allow the user to explore scalability vs accuracy trade-offs.

4. A synchronization module based on Argonne's existing work is chosen. Usually, there is one transmission simulator coupled with multiple distribution feeders, each simulated by an individual and independent distribution simulator. Argonne has developed a synchronization server that synchronizes different simulators. The synchronization server will be added on the transmission simulator side, and each distribution simulator will run on a dedicated port and register as a client of the synchronization server for synchronization calls.

The technical approach to the tool development process includes the following steps:

1. Identify the transmission simulator's application programming interface (API) and interval for information exchange.

2. Identify the distribution simulator's API and interval for information exchange.

3. Adapt Argonne's interface module, including the communication sockets, to seamlessly receive and send information between T&D simulators through their respective APIs. This interface should be able to convert between three-phase quantities and positive-sequence quantities.

4. Implement both tightly coupled and loosely coupled protocols in the interface module for information exchange between T&D simulators.

5. Add and adapt Argonne's synchronization server module to the chosen T&D simulators through their respective APIs.

6. Develop use cases to validate the accuracy of the tool and examine its usefulness in facilitating BES reliability studies.

7. Validate the tool through benchmarking with other T&D simulation software.

8. Conduct analysis based on the developed use cases to demonstrate the efficacy of the tool.

REFERENCES

[1] C. Marcy, "Renewable generation capacity expected to account for most 2016 capacity additions," https://www.eia.gov/todayinenergy/detail.php?id=29492, accessed January, 2017.

[2] California Energy Commission, "California Renewable Energy Overview and Programs," http://www.energy.ca.gov/renewables/.

[3] H. Nikkhajoei and R. Iravani, "Steady-state model and power flow analysis of electronically-coupled distributed resource units," IEEE Trans. Power Del., vol. 22, no. 1, Jan. 2007, pp. 721–728.

[4] H. Chen, J. Chen, D. Shi, and X. Duan, "Power flow study and voltage stability analysis for distribution systems with distributed generation," IEEE Power Eng. Soc. General Meeting, Montreal, QC, Canada, 2006.

[5] W. Bo, W. Sheng, L. Hua, and X. Hua, "Steady-state model and power flow analysis of grid connected photovoltaic power system," in Proc. IEEE International Conference on Industrial Technology, 2008, pp. 1–6.

[6] M. Z. Kamh and R. Iravani, "Unbalanced model and power-flow analysis of microgrids and active distribution systems," IEEE Trans. Power Del., vol. 25, no. 4, Oct. 2010, pp. 2851–2858.

[7] M. Z. Kamh and R. Iravani, "Steady-state model and power-flow analysis of single-phase electronically coupled distributed energy resources," IEEE Trans. Power Del., vol. 27, no. 1, Jan. 2012, pp. 131–139.

[8] S. Bhattacharya, T. Saha, and M. J. Hossain, "Fault current contribution from photovoltaic systems in residential power networks," Australasian Universities Power Engineering Conference, AUPEC 2013, Hobart, TAS, Australia, 29 September–3 October 2013.

[9] Institute of Electrical and Electronics Engineers (IEEE), "IEEE Standard for Interconnecting Distributed Resources with Electric Power Systems," IEEE Std. 1547-2003, July 2003, pp. 1–28.

[10] FERC, Small Generator Interconnection Procedures (SGIP) (For Generating Facilities No Larger Than 20 MW). RM13-2-000. September 19, 2009.

[11] ———, Small Generator Interconnection Agreement (SGIA) (For Generating Facilities No Larger Than 20 MW). RM13-2-000. September 19, 2009.

[12] California Public Utility Commission, "Electric Rule No. 21: Generating Facility Interconnections," http://www.pge.com/tariffs/tm2/pdf/ELEC_RULES_21.pdf, accessed April 24, 2012.

[13] Institute of Electrical and Electronics Engineers (IEEE), "IEEE Standard for Interconnecting Distributed Resources with Electric Power Systems," IEEE Std. 1547a-2014, May 2014.

[14] IEEE Standards Coordinating Committee 21, "1547 - IEEE Draft Standard for Interconnection and Interoperability of Distributed Energy Resources with Associated Electric Power Systems Interfaces," IEEE P1547/D3, 2016.

[15] FERC, Requirements for Frequency and Voltage Ride Through Capability of Small Generating Facilities: Notice of Proposed Rulemaking (NOPR). Docket No. RM16-8-000. March 17, 2016.

[16] California Public Utilities Commission, Interim Decision Adopting Revisions to Electric Tariff Rule 21 For Pacific Gas and Electric Company, Southern California Edison Company, and San Diego Gas & Electric Company to Require "Smart" Inverters. COM/MP6/lil. December 18, 2014.

[17] German Government, Verordnung zu Systemdienstleistungen durch Windenergieanlagen (Systemdienstleistungsverordnung – SDLWindV) ("Ordinance for Ancillary Services of Wind Power Plants [Ancillary Services Ordinance – SDLWindV]),," Federal Law Gazette Vol. I, No. 39 (2009), pp. 1734-1746.

[18] WECC Renewable Energy Modeling Task Force, WECC Solar Power Plant Dynamic Modeling Guidelines. Western Electricity Coordinating Council, April 2014.

[19] P. Kundur, N.J. Balu, and M.G. Lauby, Power System Stability and Control. EPRI Power System Engineering Series. McGraw-Hill, 1994.

[20] "IEEE 34 Node Test Feeder," http://ewh.ieee.org/soc/pes/dsacom/testfeeders/index.html, accessed June 23, 2017.

[21] G. H. Bode and D. G. Holmes, "Implementation of three level hysteresis current control for a single phase voltage source inverter," in 2000 IEEE 31st Annual Power Electronics Specialists Conference, Conference Proceedings (Cat. No.00CH37018), vol. 1, 2000, pp. 33–38.

[22] N. Akel, M. Pahlevaninezhad, and P. Jain, "A d-q rotating frame reactive power controller for single-phase bi-directional converters," in Proc. 2014 IEEE 36th International Telecommunications Energy Conference (INTELEC), Sept. 2014, pp. 1–5.

[23] D. W. P. Thomas and M. S. Woolfson, "Evaluation of frequency tracking methods," IEEE Trans. Power Del., vol. 16, 2001, pp. 367–371.

[24] M. M. Begovic, P. M. Duric, S. Dunlop, and A. G. Phadke, “Frequency tracking in power networks in the presence of harmonics,” IEEE Trans. Power Del., vol. 8, April 1993, pp. 480–485.

[25] A. G. Phadke, J. S. Thorp, and M. G. Adamiak, “A new measurement technique for tracking voltage phasors, local system frequency and rate of change of frequency,” IEEE Trans. Power Appl. Syst., vol. 102, 1983, pp. 1025–1038.

[26] J. Z. Yang and C. W. Liu, “A precise calculation of power system frequency,” IEEE Trans. Power Del., vol. 16, no. 3, 2001, pp. 361–366.

[27] R. Jinfeng and M. Kezunovic, “A hybrid method for power system frequency estimation,” IEEE Trans. Power Del., vol. 27, 2012, pp. 1252–1259.

[28] J. K. Hwang and Y. Liu, “Noise analysis of power system frequency estimated from angle difference of discrete Fourier transform coefficient,” IEEE Trans. Power Del., vol. 29, no. 4, Aug. 2014, pp. 1533–1541.

[29] D. Hart et al., “A new frequency tracking and phasor estimation algorithm for generator protection,” IEEE Trans. Power Del., vol. 12, no. 3, 1997, pp. 1064–1073.

[30] M. Wang and Y. Sun, “A practical, precise method for frequency tracking and phasor estimation,” IEEE Trans. Power Del., vol. 19, 2004, pp. 1547–1552.

[31] P. Denys, C. Counan, L. Hossenlopp, and C. Holweck, “Measurement of voltage phase for the French future defence plan against losses of synchronism,” IEEE Trans. Power Del., vol. 7, 1992, pp. 62–69.

[32] M. Akke, “Frequency estimation by demodulation of two complex signals,” IEEE Trans. Power Del., vol. 12, 1997, pp. 157–163.

[33] P. J. Moore, R. D. Carranza, and A. T. Johns, “A new numeric technique for high-speed evaluation of power system frequency,” IEE Proc. Gener. Transm. Distrib., vol. 141, 1994, pp. 529–536.

[34] T. S. Sidhu, “Accurate measurement of power system frequency using a digital signal processing technique,” IEEE Trans. Instr. Meas., vol. 48, no. 1, 1999, pp. 75–81.

[35] J. Szafran and W. Rebizant, “Power system frequency estimation,” IEE Proc. Gener. Transm. Distrib., vol. 145, no. 5, 1998, pp. 578–582.

[36] M. S. Sachdev and M. M. Giray, “A least error squares technique for determining power system frequency,” IEEE Trans. Power Appar. Syst., vol. 104, no. 2, 1985, pp. 435–444.

[37] M. S. Sachdev and M. Nagpal, “A recursive least error squares algorithm for power system relaying and measurement applications,” IEEE Trans. Power Del., vol. 6, no. 3, 1991, pp. 1008–1015.

[38] A. K. Pradhan et al., “Power system frequency estimation using least mean square technique,” IEEE Trans. Power Del., vol. 20, 2005, pp. 1812–1816.

[39] A. A. Girgis and T. L. D. Hwang, “Optimal estimation of voltage phasor and frequency deviation using linear and non-linear Kalman filtering: theory and limitations,” IEEE Trans. Power Appar. Syst., vol. 103, no. 10, 1984, pp. 2943–2949.

[40] P. K. Dash et al., “Frequency estimation of distorted power system signals using extended complex Kalman filter,” IEEE Trans. Power Del., vol. 14, no. 3, 1999, pp. 761–766.

[41] V. Terzija et al., “Voltage phasor and local system frequency estimation using Newton type algorithm”, IEEE Trans. Power Del., vol. 9, no. 3, 1994, pp. 1368–1374.

[42] J. Zheng, K. W. K. Lui, W. K. Ma, and H. C. So, “Two simplified recursive Gauss–Newton algorithms for direct amplitude and phase tracking of a real sinusoid,” IEEE Signal Process. Lett., vol. 14, 2007, pp. 972–975.

[43] S. Y. Xue and S. X. Yang, “Power system frequency estimation using supervised Gauss-Newton algorithm,” Measurement, vol. 42, no. 1, 2009, pp. 28–37.

[44] P. K. Dash, K. R. Krishnanand, and R. K. Patnaik, “Dynamic phasor and frequency estimation of time-varying power system signals,” Intl. J. Electr. Power Energy Syst., vol. 44, 2013, pp. 971–980.

[45] L. L. Lai, W. L. Chan, C. T. Tse, and A. T. P. So, “Real-time frequency and harmonic evaluation using artificial neural networks,” IEEE Trans. Power Del., vol. 14, no. 1, 1999, pp. 52–59.

[46] P. K. Dash, D. P. Swain, A. Routray, and A. C. Liew, “An adaptive neural network approach for the estimation of power system frequency,” Electr. Power Syst. Res., vol. 41, 1997, pp. 203–210.

[47] Z. Zhong et al., “Power system frequency monitoring network (FNET) implementation,” IEEE Trans. Power Syst., vol. 20, no. 4, Nov. 2005, pp. 1914–1921.

[48] R. Singh, B. C. Pal, and R. A. Jabr, “Statistical representation of distribution system loads using Gaussian mixture model,” IEEE Trans. Power Syst., vol. 25, no. 1, Feb. 2010, pp. 29–37.

[49] W. H. Kersting, “Radial distribution test feeders,” in Proc. Power Engineering Society Winter Meeting, IEEE, vol. 2, 2001, pp. 908–912.

[50] "IEEE 13 Node Test Feeder," http://ewh.ieee.org/soc/pes/dsacom/testfeeders/index.html, accessed June 23, 2017.

[51] "Three Phase PI Section Line," https://www.mathworks.com/help/physmod/sps/powersys/ref/threephasepisectionline.html, accessed June 23, 2017.

[52] W. Liu, L. Chen, J. Ou, and S. Cheng, "Simulation of PMSG wind turbine system with sensor-less control technology based on model reference adaptive system," in 2011 International Conference on Electrical Machines and Systems (ICEMS), IEEE, 2011, pp. 1–3.

[53] J. Slootweg, H. Polinder, and W. Kling, "Representing wind turbine electrical generating systems in fundamental frequency simulations," IEEE Trans. Energy Conv., vol. 18, no. 4, 2003, pp. 516–524.

This page intentionally left blank.

Energy Systems Division
9700 South Cass Avenue, Bldg. 362
Argonne, IL 60439-4854

www.anl.gov